Clim Dyn (2013) 40:3107–3134
DOI 10.1007/s00382-012-1569-8

The global energy balance from a surface perspective

Martin Wild · Doris Folini · Christoph Schär · Norman Loeb · Ellsworth G. Dutton · Gert König-Langlo

Received: 31 July 2012 / Accepted: 12 October 2012 / Published online: 13 November 2012
© Springer-Verlag Berlin Heidelberg 2012

Abstract In the framework of the global energy balance, the radiative energy exchanges between Sun, Earth and space are now accurately quantified from new satellite missions. Much less is known about the magnitude of the energy flows within the climate system and at the Earth surface, which cannot be directly measured by satellites. In addition to satellite observations, here we make extensive use of the growing number of surface observations to constrain the global energy balance not only from space, but also from the surface. We combine these observations with the latest modeling efforts performed for the 5th IPCC assessment report to infer best estimates for the global mean surface radiative components. Our analyses favor global mean downward surface solar and thermal radiation values near 185 and 342 Wm^{-2}, respectively, which are most compatible with surface observations. Combined with an estimated surface absorbed solar radiation and thermal emission of 161 and 397 Wm^{-2}, respectively, this leaves 106 Wm^{-2} of surface net radiation available globally for distribution amongst the non-radiative surface energy balance components. The climate models overestimate the downward solar and underestimate the downward thermal radiation, thereby simulating nevertheless an adequate global mean surface net radiation by error compensation. This also suggests that, globally, the simulated surface sensible and latent heat fluxes, around 20 and 85 Wm^{-2} on average, state realistic values. The findings of this study are compiled into a new global energy balance diagram, which may be able to reconcile currently disputed inconsistencies between energy and water cycle estimates.

Keywords Earth Radiation Budget · Surface energy balance · Global climate models · Global energy balance · Surface/Satellite observations · CMIP5/IPCC-AR5 model evaluation

M. Wild (✉) · D. Folini · C. Schär
Institute for Atmospheric and Climate Science, ETH Zurich, Universitätsstr. 16, 8092 Zurich, Switzerland
e-mail: martin.wild@env.ethz.ch

N. Loeb
NASA Langley Research Center, 21 Langley Boulevard, Hampton, VA 23681-2199, USA

E. G. Dutton
NOAA/ESRL, R/GMD, 325 Broadway, Boulder, CO 80305, USA

G. König-Langlo
Alfred Wegener Institute, Bussestrasse 24, 27570 Bremerhaven, Germany

1 Introduction

The genesis and evolution of Earth's climate is largely regulated by the global energy balance and its spatial and temporal variations. Anthropogenic climate change is, from a physical point of view, first of all a perturbation of the energy balance of the globe, through the modification of the atmospheric composition of greenhouse gases and aerosols. Variations in the global energy balance affect not only the thermal conditions on the planet, but also various other climate elements, such as atmospheric and oceanic circulations, the components of the hydrological cycle, glaciers, plant productivity, and terrestrial carbon uptake (e.g., Ramanathan et al. 2001; Ohmura et al. 2007; Mercado et al. 2009; Wild et al. 2008). Despite the central role of the global energy balance in the climate system, substantial uncertainties exist in the quantification of its different components, and its representation in climate models, as pointed out

in numerous studies published over the past decades (e.g., Hartmann and Short 1980; Hartmann et al. 1986; Ramanathan et al. 1989; Gutowski et al. 1991; Ohmura and Gilgen 1993; Pinker et al. 1995; Li et al. 1997; Gleckler and Weare 1997; Kiehl and Trenberth 1997; Wild et al. 1998; Gupta et al. 1999; Hatzianastassiou and Vardavas 1999; Potter and Cess 2004; Raschke and Ohmura 2005; Trenberth et al. 2009; Trager-Chatterjee et al. 2010; Ohmura 2012; Qian et al. 2012; Wild 2012; Stephens et al. 2012a, b). This becomes also evident when comparing different schematic diagrams of the global energy balance published in text books or in the peer-reviewed literature, which often vary greatly in the numbers given therein representing the magnitudes of these energy flows in terms of global means (e.g., Kiehl and Trenberth 1997; Trenberth et al. 2009; Wild et al. 1998; Raschke and Ohmura 2005; Wild 2012; Stephens et al. 2012b). A representation of such an energy balance diagram is given in Fig. 1 and will be discussed in more detail in this study.

Knowledge on the energy exchange between Sun, Earth and space has recently been improved through new satellite missions such as the Clouds and the Earth's Radiant Energy System (CERES, Wielicki et al. 1996) and the Solar Radiation and Climate Experiment (SORCE, Anderson and Cahalan 2005). These allow the determination of the top of atmosphere (TOA) radiative flux exchanges with unprecedented accuracy (Loeb et al. 2012).

Much less is known, however, about the energy distribution *within* the climate system and at the Earth surface. Unlike the fluxes at the TOA, the surface fluxes cannot be directly measured by satellites. Instead, they have to be inferred from the measurable TOA radiances using empirical or physical models to account for atmospheric attenuation and emission, which introduces additional uncertainties. Uncertainties in the components of the surface radiation budget are thus generally larger and less well quantified than at the TOA. Debated are, for example, the partitioning of solar energy absorption between the atmosphere and surface, as well as the determination of the thermal energy exchanges at the surface/atmosphere interface (e.g., Raschke and Ohmura 2005; Wild 2008, 2012; Trenberth et al. 2009; Stephens et al. 2012b).

In the present study, we do not only rely on satellite observations, but make extensive use of the information contained in radiation measurements taken from the Earth surface, to provide direct observational constraints also for the surface fluxes. Such observations become increasingly available from ground-based radiation networks (Sect. 2). We use these observations to assess the radiation budgets as simulated in the latest modeling efforts performed within

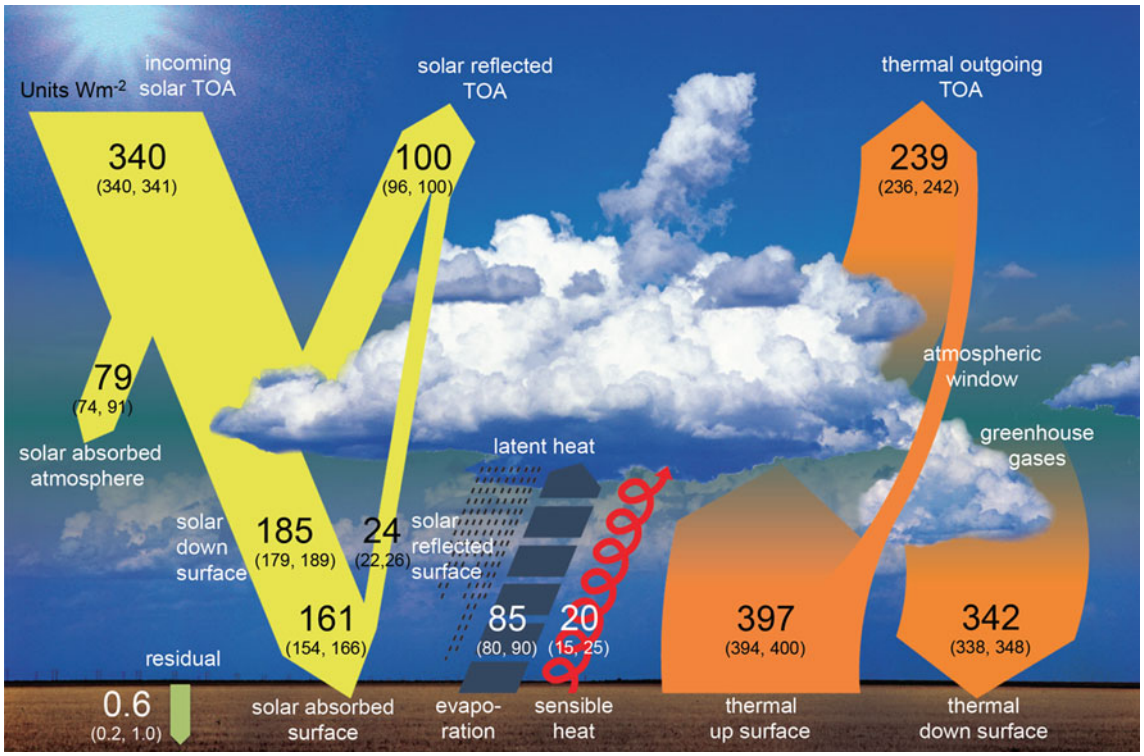

Fig. 1 Schematic diagram of the global mean energy balance of the Earth. *Numbers* indicate best estimates for the magnitudes of the globally averaged energy balance components together with their uncertainty ranges, representing present day climate conditions at the beginning of the twenty first century. Estimates and uncertainty ranges based on discussion in Sect. 5. Units Wm^{-2}

the Coupled Model Intercomparison Project Phase 5 (CMIP5) for the upcoming 5th IPCC assessment report (IPCC-AR5) (Sects. 3, 4). We further combine the surface observations with these models to infer best estimates of the global mean surface radiative components (Sect. 4). The outcome of this study is used to discuss a new global energy balance diagram (Fig. 1), which incorporates the best estimates for the surface energy flux components derived here along with recent best estimates for the TOA flux components (Sect. 5). Conclusions are drawn in Sect. 6.

2 Observational data

The satellite observations used in this study to constrain the net fluxes at the TOA stem from the CERES mission that measures filtered radiances in the solar (0.3 and 5 μm), total (0.3 and 200 μm), and window (8 and 12 μm) regions (Wielicki et al. 1996). Since there is no thermal channel on CERES, thermal daytime radiances are determined from the difference between the total and solar channel radiances. The global mean estimates for the components of the TOA radiation budget are based on the energy balanced and filled (EBAF) data set for the period 2001–2010 as part of the CERES mission, version EBAF 2.6r (Loeb et al. 2012). This data set adjusts the solar and thermal TOA fluxes within their range of uncertainty to be consistent with independent estimates of the global heating rate based upon in situ ocean observations (Loeb et al. 2009).

The surface observations to constrain the surface radiative fluxes are retrieved from two data sources: The global energy balance archive (GEBA, Gilgen et al. 1998; Ohmura et al. 1989) and the database of the Baseline Surface Radiation Network (BSRN, Ohmura et al. 1998). GEBA is a database for the worldwide measured energy fluxes at the Earth's surface and currently contains 2,500 stations with 450,000 monthly mean values of various surface energy balance components. GEBA is maintained at ETH Zurich. By far the most widely measured quantity is the solar radiation incident at the Earth's surface, also known as global radiation, and referred to as downward solar radiation in the following. Gilgen et al. (1998) estimated the relative random error (root mean square error/mean) of the downward solar radiation values in GEBA at 5 % for the monthly means and 2 % for yearly means. A subset of 760 GEBA sites, which provide multiyear records and allow the construction of representative solar radiation climatologies, was used in the present study. This dataset has been used in previous studies for climate model validation and therefore allows a comparison of the performance of the latest models in the present study with older model versions which use the same observational reference (e.g., Wild 2008). Further, a small set of records of downward thermal radiation is contained in GEBA, which is also used in this study.

BSRN provides radiation measurements with high accuracy and temporal resolution (minute data) at a limited number of sites in various climate zones. First BSRN sites became operational in the early 1990s. To date more than 50 anchor sites in various climate regimes have reported their data to the BSRN Archive at the Alfred Wegener Institute (AWI) (http://www.bsrn.awi.de/). The accuracy of downward thermal radiation measurements, carried out with pyrgeometers, is near 3–4 Wm^{-2} according to Philipona et al. (2001) and Marty et al. (2003), thereby meeting BSRN standards established by Ohmura et al. (1998). The downward shortwave radiation at the BSRN sites is required to be measured both as a single total flux measurement with a pyranometer and as component sum of separate measurements of the direct shortwave flux (measured with a pyrheliometer) and the diffuse shortwave flux (measured with a shaded pyranometer). A pyranometer measures the total incoming solar radiation in the wavelengths between 0.3 and 2.8 μm. Datasets from both measurement methods are used in this study. Some pyranometers used are known to have instantaneous accuracy limitations of 3–5 % of the full signal due to cosine response and thermal offset errors combined with other sources of uncertainty. However, using single pyranometers in conjunction with the component sum method at BSRN sites (Michalsky et al. 1999), and considering long term averaging, an accuracy near 5 Wm^{-2} ($\sim$2 % for 24-h mean solar irradiance) has been achieved, meeting the BSRN specifications under optimal observing conditions. The enhanced accuracy of the component sum is supported by recent work (Michalsky et al. 2011) that demonstrated typical operational pyrheliometer measurement instantaneous accuracy to be 0.7–1.3 % (95 % confidence level) and by earlier work (Michalsky et al. 2007), demonstrating the instantaneous accuracy of near-zero-offset pyranometers to be better than 2–4 Wm^{-2} when used for diffuse (shaded) solar measurements (note that instantaneous solar irradiance measurement uncertainties in terms of Wm^{-2} are reduced, typically by about a factor of 2, when using 24-h or longer averaging). All BSRN solar measurements are referenced to the World Radiation Reference (WRR) scale (Frohlich 1991) and as subsequently maintained at the World Radiation Center, Davos, Switzerland, considered to be accurate to within 0.3 % and has demonstrated stability to better than 0.01 % over the past three and half decades. The WRR is based on a group of absolute cavity radiometers of similar to identical design as those used to initially establish the consensus nominal solar "constant" of 1,365 Wm^{-2}. Therefore, to make the BSRN measurements consistent with models and other analysis using a

new solar constant of 1,360.8 Wm^{-2} requires lowering the BSRN reported surface solar irradiance values by 0.3 %.

Out of the 50 BSRN sites, more than 40 sites already provide multiyear records which allow a determination of representative radiation climatologies. They cover at least a portion of the BSRN period 1992–2011, and thus can be considered as representing present-day climate conditions around the turn of the century. For the present study we were able to use pyranometer records from 42 stations, combined pyrheliometer and shaded pyranometer records from 38 stations, and pyrgeometer data from 41 stations. Due to the necessity to track the sun with the pyrheliometer and the shading disk, data gaps in the direct and diffuse records are typically more frequent than with the pyranometer measurements, which explains the slightly lower number of stations available for climatologies based on combined direct and diffuse measurements. A list of the BSRN stations used in this study is given in Table 1. The geographical distribution of the GEBA and BSRN sites used in this study is displayed in Fig. 2.

Monthly mean values were calculated from the BSRN minute raw data as described in Roesch et al. (2011), by determining for each month first a mean monthly diurnal cycle from the raw data gathered into 15-min bins, and then averaging over the 24 h' cycle to obtain a monthly mean. This method minimizes the risk of biases in monthly means calculated from incomplete data records.

3 Model data

We make use of general circulation model (GCM) generated data that have been compiled in the framework known as CMIP5 (5th phase of the Coupled Model Intercomparison Project). These data have been organized by the Program for Climate Model Diagnosis and Intercomparison (PCMDI) for the 5th IPCC assessment report. We focus on the "historical" experiments therein. These experiments were aimed at reproducing the climate evolution of the twentieth century as accurately as possible, by considering all major natural and anthropogenic forcings, such as changes in atmospheric greenhouse gases, aerosol loadings (tropospheric and stratospheric volcanic), solar output, and land use. These experiments are therefore best suited for the assessment of the capability of the models to reproduce the global energy balance as accurately as possible. Most experiments start around 1860 and are carried out up to around 2005. We analyzed the last 2 decades of these experiments (1985–2004) which are completely covered by all participating models. This period can be considered as representative for present day climate conditions and is long enough to generate stable climatological means. We also tested our analyses with differing start and end years, but found the results presented in this study insensitive to the choice of the period. This is also understandable given the lack of decadal variations in the surface radiative fluxes calculated in the models (Wild and Schmucki 2011). As of June 2012, historical experiments from 22 models were available from PCMDI for our analyses. These models are listed in Table 2, together with their respective home institutions. A detailed description of these models is provided on the web pages of the PCMDI (http://www-pcmdi.llnl.gov/). Most participating groups performed multiple simulations of this historic period with differing initial conditions (ensemble experiments). However, we found that within our analyses, the choice of a particular ensemble member from a specific model hardly influenced the results and played a minor role. Therefore, we only consider one ensemble realization of each model in the following analyses.

In addition to the CMIP5 models, surface radiative fluxes as estimated in the reanalysis from the European Centre for Medium-Range Weather Forecasts (ECMWF) covering the period 1958–2002 (ERA40, Uppala et al. 2005) are considered in this study. Reanalyses assimilate the comprehensive worldwide observations from the global observing system (GOS) into their models. They do not, however, assimilate the surface radiation observations used in this study.

4 Assessment with direct observations

4.1 TOA radiation budgets

As mentioned in the introduction, the TOA radiative flux exchanges are now known with unprecedented accuracy from recent satellite programs such as CERES and SORCE. The total solar irradiance (TSI) incident at the TOA, based on the most recently launched SORCE Total Irradiance Monitor (TIM), is determined at 1360.8 ± 0.5 Wm^{-2} (annual mean), with reported uncertainties as low as 0.035 % (Kopp et al. 2005; Kopp and Lean 2011). This value is lower than previous estimates, which were around 1,365 Wm^{-2} (Kopp and Lean 2011). Distributed over the sphere of the globe this revised estimate corresponds to a total solar irradiance close to 340 Wm^{-2}, with an uncertainty range of less than 1 Wm^{-2}. The GCMs typically still use the older, somewhat higher TSI, thus showing a multimodel mean of 341.2 Wm^{-2}, with a standard deviation of 0.7 Wm^{-2} (Table 3). Specifically, 16 out of 22 models use a value in the small range between 341.4 and 341.6 Wm^{-2}, 5 models a value of 340.4 Wm^{-2} close to the SORCE estimate, and one model a lower value of 338.9 Wm^{-2}. This signifies that the majority of the GCMs calculate slightly too much solar irradiance at the TOA compared to the latest estimates, on the order of 1 Wm^{-2} globally.

Table 1 BSRN stations used in this study, with their abbreviation and geographical location and elevation above sea level (in m)

Station name	Abbreviation	Location	Latitude	Longitude	Altitude
Alice Springs	ASP	Australia	−23.798	133.888	547
Barrow	BAR	Alaska, USA	71.323	156.607	8
Bermuda	BER	Bermuda	32.267	−64.667	8
Billings	BIL	Oklahoma, USA	36.605	−97.516	317
Bondville	BON	Illinois, USA	40.066	−88.367	213
Boulder	BOS	Colorado, USA	40.125	−105.237	1,689
Boulder	BOU	Colorado, USA	40.050	−105.007	1,577
Cabauw	CAB	The Netherlands	51.971	4.927	0
Camborne	CAM	United Kingdom	50.217	−5.317	88
Carpentras	CAR	France	44.083	5.059	100
Cener	CNR	Spain, Sarriguren, Navarra	42.816	−1.601	471
Chesapeake Light	CLH	North Atlantic Ocean	36.905	−75.713	37
Cocos Island	COC	Cocos (Keeling) Islands	−12.193	96.835	0
Darwin	DAR	Australia	−12.425	130.891	30
Darwin Met Office	DWN	Australia	−12.424	130.892	32
De Aar	DAA	South Africa	−30.667	23.993	1,287
Desert Rock	DRA	Nevada, USA	36.626	−116.018	1,007
Florianopolis	FLO	Brazil	−27.533	−48.517	11
Fort Peck	FPE	Montana, USA	48.317	−105.100	634
Georg von Neumayer	GVN	Antarctica	−70.650	−8.250	42
Goodwin Creek	GCR	Mississippi, USA	34.250	−89.870	98
Ilorin	ILO	Nigeria	8.533	4.567	350
Ishigakijima	ISH	Japan	24.337	124.163	6
Izaña	IZA	Tenerife, Spain	28.309	−16.499	2,373
Kwajalein	KWA	North Pacific Ocean	8.720	167.731	10
Lerwick	LER	United Kingdom	60.133	−1.183	84
Lindenberg	LIN	Germany	52.210	14.122	125
Momote	MAN	Papua New Guinea	−2.058	147.425	6
Nauru Island	NAU	Nauru	−0.521	166.917	7
Ny-Ålesund	NYA	Ny-Ålesund, Spitsbergen	78.925	11.930	11
Palaiseau	PAL	France	48.713	2.208	156
Payerne	PAY	Switzerland	46.815	6.944	491
Regina	REG	Canada	50.205	−104.713	578
Rock Springs	PSU	Pennsylvania, USA	40.720	−77.933	376
S. Great Plains	E13	Oklahoma, USA	36.605	−97.485	318
Sede Boqer	SBO	Israel	30.905	34.782	500
Sioux Falls	SXF	South Dakota, USA	43.730	−96.620	473
Solar Village	SOV	Saudi Arabia	24.910	46.410	650
South Pole	SPO	Antarctica	−89.983	−24.799	2,800
Syowa	SYO	Cosmonaut Sea	−69.005	39.589	18
São Martinho da Serra	SMS	Brazil	−29.443	−53.823	489
Tamanrasset	TAM	Algeria	22.780	5.510	1,385
Tateno	TAT	Japan	36.050	140.133	25
Toravere	TOR	Estonia	58.254	26.462	70
Xianghe	XIA	China	39.754	116.962	32

According to the CERES EBAF satellite data product (Loeb et al. 2009), the global mean reflected shortwave TOA flux for the period 2001–2010 amounts to 100 Wm^{-2}, with a stated uncertainty in absolute calibration alone of $\sim$2 % (2-sigma), corresponding to 2 Wm^{-2}. The EBAF data set adjusts the solar and thermal TOA

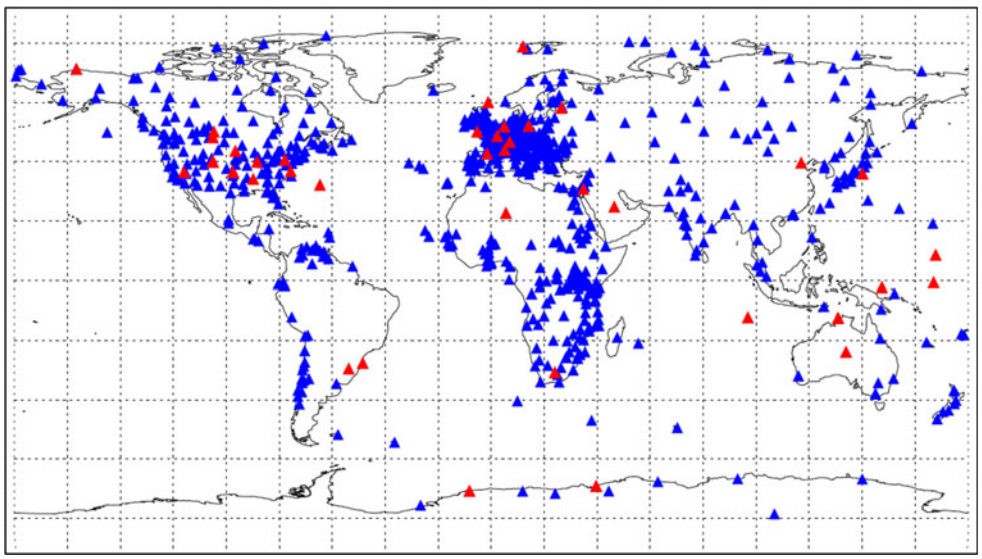

Fig. 2 Geographical distribution of observation sites used in this study from GEBA (760 sites in blue), and from BSRN (42 sites in red, c.f. Table 1)

fluxes within their range of uncertainty to be consistent with independent estimates of the global heating rate based upon in situ ocean observations (Loeb et al. 2012; Loeb et al. 2009). The 100 Wm^{-2} adjusted in this way are at the upper end of this uncertainty range which spans from 96 to 100 Wm^{-2} (Loeb et al. 2009). The 100 Wm^{-2} reflected solar radiation leaves 240 Wm^{-2} as the best estimate for the amount of solar radiation globally absorbed by the climate system. The global mean absorbed solar radiation in the climate system (net solar radiation at the TOA) calculated in the 22 models is shown in Fig. 3 (uppermost panel). The mean and median of all models shown in this Figure amounts to 238.9 and 239.5 Wm^{-2}, respectively, with a standard deviation of 3.0 Wm^{-2} (Table 3) and is well within the observational uncertainty range. The close agreement of the GCMs with the satellite estimate from CERES EBAF is not surprising, since the cloud schemes of the GCMs are usually tuned to match the satellite reference values on a global mean basis. Overall, there seems no obvious systematic bias in the CMIP5 models compared to the satellite reference value, although individual models deviate from the CERES best estimate of 240 Wm^{-2} by up to 6 Wm^{-2} (Table 3; Fig. 3 uppermost panel).

The 240 Wm^{-2} of solar radiation absorbed by the globe are nearly balanced by thermal emission to space (also known as outgoing longwave radiation) of about 239 Wm^{-2}. This value is based on CERES EBAF, taking into account an energy imbalance at the TOA of approx. 0.6 Wm^{-2} (Hansen et al. 2011; Loeb et al. 2012). This imbalance, which reflects the global heat storage, is constrained by observations of changes in ocean heat content. Specifically, Lyman et al. 2010 determined a warming of 0.64 ± 0.11 Wm^{-2} (90 % confidence level) in the upper ocean over the period 1993–2008, which Hansen et al. (2011) translate into a planetary energy imbalance of 0.8 ± 0.2 Wm^{-2} (one sigma uncertainty). A slightly lower planetary imbalance of 0.58 Wm^{-2} is obtained by Hansen et al. (2011) for the same period, if the Levitus et al. (2009) upper ocean heat uptake estimate is used instead. Based on a combination of satellite data and ocean measurements to depths of 1,800 m, Loeb et al. (2012) estimated that Earth has been accumulating energy at a rate of 0.5 ± 0.43 Wm^{-2} between 2001 and 2010 (90 % confidence level), and of 0.58 ± 0.38 Wm^{-2} between July 2005 and June 2010, in line with the estimate given by Hansen et al. (2011) for the latter period. The planetary imbalance in the CMIP5 models around the turn of the century is on average 1.0 Wm^{-2} (median 0.9 Wm^{-2}) as can be inferred from Table 3.

The uncertainty of the outgoing thermal flux at the TOA as measured by CERES (derived from the total channel at night and the difference between the total and shortwave channels during daytime) due to calibration is ~3.7 Wm^{-2} (2-sigma). Additional uncertainty comes from unfiltering the radiances, radiance-to-flux conversion, and time–space averaging, which adds up to another 1 Wm^{-2} or more (Loeb et al. 2009). The 2-sigma uncertainty range for the global mean thermal outgoing radiation therefore spans from about 236–242 Wm^{-2}. The global mean thermal outgoing radiation as simulated by the CMIP5 models is shown in Fig. 4 (uppermost panel). The multimodel mean and median values are, at 237.9 and 238.5 Wm^{-2} respectively, within the uncertainty range of the CERES satellite reference value mentioned above. This close agreement is again largely a result of the model tuning process against satellite data. Therefore the CMIP5 model calculations cannot be considered as independent estimates for the magnitude of the TOA fluxes. Overall, there is no evidence for substantial systematic model biases in the TOA net flux exchanges in the CMIP5 models relative to CERES on a global mean basis.

Table 2 List of 22 models used in this study, together with their abbreviations and host institutions

Modelling groups	Institute ID	Model Name
Beijing Climate Center, China Meteorological Administration	BCC	BCC-CSM1.1
Canadian Centre for Climate Modelling and Analysis	CCCMA	CanESM2
National Center for Atmospheric Research	NCAR	CCSM4
Centre National de Recherches Meteorologiques/ Centre Europeen de Recherche et Formation Avancees en Calcul Scientifique	CNRM-CERFACS	CNRM-CM5
Commonwealth Scientific and Industrial Research Organization in collaboration with Queensland Climate Change Centre of Excellence	CSIRO-QCCCE	CSIRO-Mk3.6.0
NOAA Geophysical Fluid Dynamics Laboratory	NOAA GFDL	GFDL-CM3
		GFDL-ESM2G
		GFDL-ESM2 M
NASA Goddard Institute for Space Studies	NASA GISS	GISS-E2-H
		GISS-E2-R
Met Office Hadley Centre	MOHC	HadCM3
		HadGEM2-CC
		HadGEM2-ES
Institute for Numerical Mathematics	INM	INM-CM4
Institut Pierre-Simon Laplace	IPSL	IPSL-CM5A-LR
		IPSL-CM5A-MR
Japan Agency for Marine-Earth Science and Technology, Atmosphere and Ocean Research Institute (The University of Tokyo), and National Institute for Environmental Studies	MIROC	MIROC4h
		MIROC5
		MIROC-ESM
Max Planck Institute for Meteorology	MPI-M	MPI-ESM-LR
Meteorological Research Institute	MRI	MRI-CGCM3
Norwegian Climate Centre	NCC	NorESM1-M

4.2 Surface radiation budgets

In contrast to the fluxes at the TOA, generally accepted observational reference values for the globally averaged surface downwelling fluxes, which could be used for a simple comparison with the model-calculated global mean fluxes, are still lacking. However, the downward fluxes of the climate models, both in the solar and thermal spectral range, can be directly compared with surface observations on a site by site basis, as done in the following.

4.2.1 Solar radiation

Global mean values of downward solar radiation at Earth's surface as calculated in the CMIP5 models are shown in Fig. 5. The multimodel mean and median values are 189.4 and 189.1 Wm^{-2}, respectively (Table 3). The models show a considerable spread in this quantity and vary in a range of more than 15 Wm^{-2}, with a standard deviation of 4.2 Wm^{-2}. In the following we use the direct surface radiation observations from GEBA and BSRN to better constrain the considerable spread in the model calculated fluxes. From GEBA, we use 760 worldwide distributed stations shown in blue in Fig. 2, which provide multiyear records and adequately describe the mean present day radiation conditions at their locations (see Sect. 2). The observational dataset used here is the same as in earlier studies, to allow for a direct comparison of the results obtained here based on the CMIP5 models with the results based on earlier Atmosphere Model Intercomparison Projects (AMIPI, II) as well as the 3th phase of the Coupled Model Intercomparison Project (CMIP3) used for the 4th IPCC assessment report. For the comparison of the model-calculated fluxes with observations, the gridded model fields were interpolated to the measurement sites using the 4 surrounding grid points weighted by their inverse spherical distance.

In Fig. 6, long term annual means of downward solar radiation observed at the 760 surface sites are compared to the corresponding fluxes calculated by the various CMIP5 models. The model-calculated fluxes correlate well with their observed counterparts, with correlation coefficients ranging from 0.89 to 0.94 (Fig. 6). Note that the high correlations profit from the common strong latitudinal dependencies of both observed and simulated fluxes. Figure 7 displays for each model the long term annual mean bias in downward solar radiation at Earth's surface as average over

Table 3 Statistics on global mean solar and thermal energy balance components as calculated in 22 CMIP5/IPCC AR5 models at the TOA, in the atmosphere, and at the surface for present day climate

	Mean	Median	Min	Max	Range	Stddev
TOA components						
Solar down	341.2	341.6	338.9	341.6	2.8	0.7
Solar up	102.3	102.8	96.3	107.8	11.6	2.9
Solar net	238.9	239.5	233.8	244.7	10.9	3.0
Thermal up	237.9	238.5	232.4	243.4	11.0	2.6
Atmospheric components						
Solar net	74.0	74.0	69.7	79.1	9.4	2.6
Thermal net	179.2	179.4	171.9	194.0	22.1	4.4
Surface components						
Solar down	189.4	189.1	181.9	197.4	15.5	4.2
Solar up	24.8	24.2	20.9	31.5	10.6	2.4
Solar net	164.8	164.8	159.6	170.1	10.4	3.4
Thermal down	338.2	338.2	327.7	347.5	19.8	4.8
Thermal up	396.9	397.3	392.6	403.7	11.1	2.5
Thermal net	−58.7	−58.4	−65.2	−49.4	15.8	3.7
Net radiation	106.2	105.4	100.3	116.6	16.2	3.9
Latent heat	85.4	85.8	78.8	92.9	14.1	4.1
Sensible heat	19.4	18.7	14.5	27.7	13.2	3.1

Statistics include multimodel mean, median, minimum and maximum model values, as well as range and standard deviation of model values

the 760 GEBA sites (blue bars). Model biases range from +24 Wm^{-2} to −3 Wm^{-2}. With one exception, all models overestimate the downward solar radiation on average at the 760 sites. The multimodel mean bias averages to 10.5 Wm^{-2}, while the median bias of all models amounts to 11.1 Wm^{-2}.

Model biases in downward solar radiation as function of latitude are shown in Fig. 8. In this Figure, the displayed biases are averages over the model biases at sites located within common latitudinal belts of 5°. A few models show a maximum overestimation in the low latitudes, a feature that was common in many of the older models (c.f., Wild et al. 1998; Wild 2008). The majority of the CMIP5 models, however, do no longer exhibit a pronounced latitudinal dependency of their biases. We also determined for each model a bias, which averages over the biases in the latitude belts, weighed by the area of this latitude belt. Thus, these biases, annotated in Fig. 8, in addition account for the inhomogeneous latitudinal distribution of the sites. However, the biases obtained this way are overall very similar (multimodel mean bias 10.6 Wm^{-2}) to the biases obtained above in Figs. 6 and 7 by a simple averaging over the biases at the individual sites (multimodel mean bias 10.5 Wm^{-2}). This suggests that the mean model biases at the 760 sites are not overly sensitive to the way they are determined (i.e. by a simple averaging over all sites' biases, or by averaging over the area weighed latitudinal mean biases).

To further assess the effect of the choice of surface observation sites and measurement quality on the model biases in downward solar radiation, we repeated the above analysis with a set of 42 BSRN stations instead of the 760 GEBA sites used above. They have a different and coarser global distribution as shown in Fig. 2 (red sites) and are considered of highest quality. Nevertheless, again the results turn out similar. In Fig. 7, the red bars indicate the individual model biases as averages over the biases at the 42 BSRN sites. They largely follow the blue bars in this Figure, which state the bias of the respective models at the 760 GEBA sites. 19 out of the 22 models overestimate the downward solar radiation on average at the 42 BSRN sites (red bars in Fig. 7). The multimodel mean and median biases in the 22 CMIP5 models compared to the 42 BSRN sites amount to 8.1 and 9.2 Wm^{-2}, respectively. The observations are thereby based on pyranometer measurements at the BSRN sites. Alternatively, surface downward solar radiation can be measured by the sum of the direct radiation (measured with a pyrheliometer) and the diffuse radiation (measured with a shaded pyranometer) (see Sect. 2). This latter method (component method) is the one recommended by BSRN to measure the downward solar radiation. At 38 out of the 42 BSRN sites, the records of direct and diffuse radiation were complete enough to determine surface downward solar radiation climatologies with the component method. The model-calculated downward solar radiation biases compared to these observations are shown in Fig. 9 at the 38 individual BSRN sites. At 32 out of the 38 sites, the downward solar radiation is overestimated on average by the 22 CMIP5 models (Fig. 9). At each site in Fig. 9 one standard deviation of the individual model biases is further indicated. The overall difference to the measurements with pyranometers is only 0.15 Wm^{-2} averaged over all 38 sites which provide climatologies based on both pyranometer and diffuse/direct measurements. At individual sites, the differences in the long-term annual means measured with the two measurement methods are within a few Wm^{-2}. This suggests that the measurement method (pyranometer or component method) does not introduce systematic differences in the radiation climatologies. Thus, the model biases determined here are fairly robust with respect to the geographical distribution of the observation sites as well as with respect to the measurement technique applied. Selecting only those BSRN sites that are located in the oceans on small islands (Cocos Island, Kwajalein, Momote, Nauru Island, Chesapeake Lighthouse, Bermudas, cf. Table 1), shows an average overestimation of downward solar radiation by the CMIP5 models of 8 Wm^{-2}, which is similar to the overall overestimation at all BSRN sites. This suggests that there are no obvious systematic differences in the model biases between sites located over land and oceans.

Mean annual cycles at the 38 BSRN sites as calculated by the individual models and as measured by the component

Fig. 3 Global annual mean solar radiation budgets calculated by 22 CMIP5/IPCC AR5 models for present day climate. Solar radiation absorbed at the surface (*lowermost panel*), within the atmosphere (*middle panel*), and in the total climate system (TOA, *uppermost panel*). Units Wm^{-2}

method are indicated in Fig. 10 as red and black lines, respectively. It further illustrates that the majority of the models overestimates the downward solar radiation throughout the year at many of the BSRN sites. The maximum overestimation is predominantly found in the summer season with maximum absolute amounts of radiation, while the overestimation in the winter season with minimum absolute amounts of radiation is less pronounced. Quantitatively, the month with maximum downward solar radiation (peak summer month) averaged over all stations and models is 16 Wm^{-2} higher than observed, while the month with minimum downward solar radiation (peak winter month) is 2 Wm^{-2} larger than observed when averaged over all sites and models.

The overestimation of surface solar irradiance is a long-standing problem in climate modeling. It has been documented in previous assessments of older models and in earlier model intercomparison projects (AMIPI, II and CMIP3), which revealed similar or larger biases (e.g., Garratt 1994; Wild et al. 1995b; Li et al. 1997; Morcrette 2002; Wild 2005; Bodas-Salcedo et al. 2008; Markovic et al. 2008; Wild 2008). In Table 4, for those institutions that took part in both CMIP3 and CMIP5, biases in their CMIP3 model versions are compared with the respective biases of their successor versions in CMIP5, based again on averaging the model biases at the 760 GEBA sites. Table 4 illustrates that there is no clear tendency towards reduced

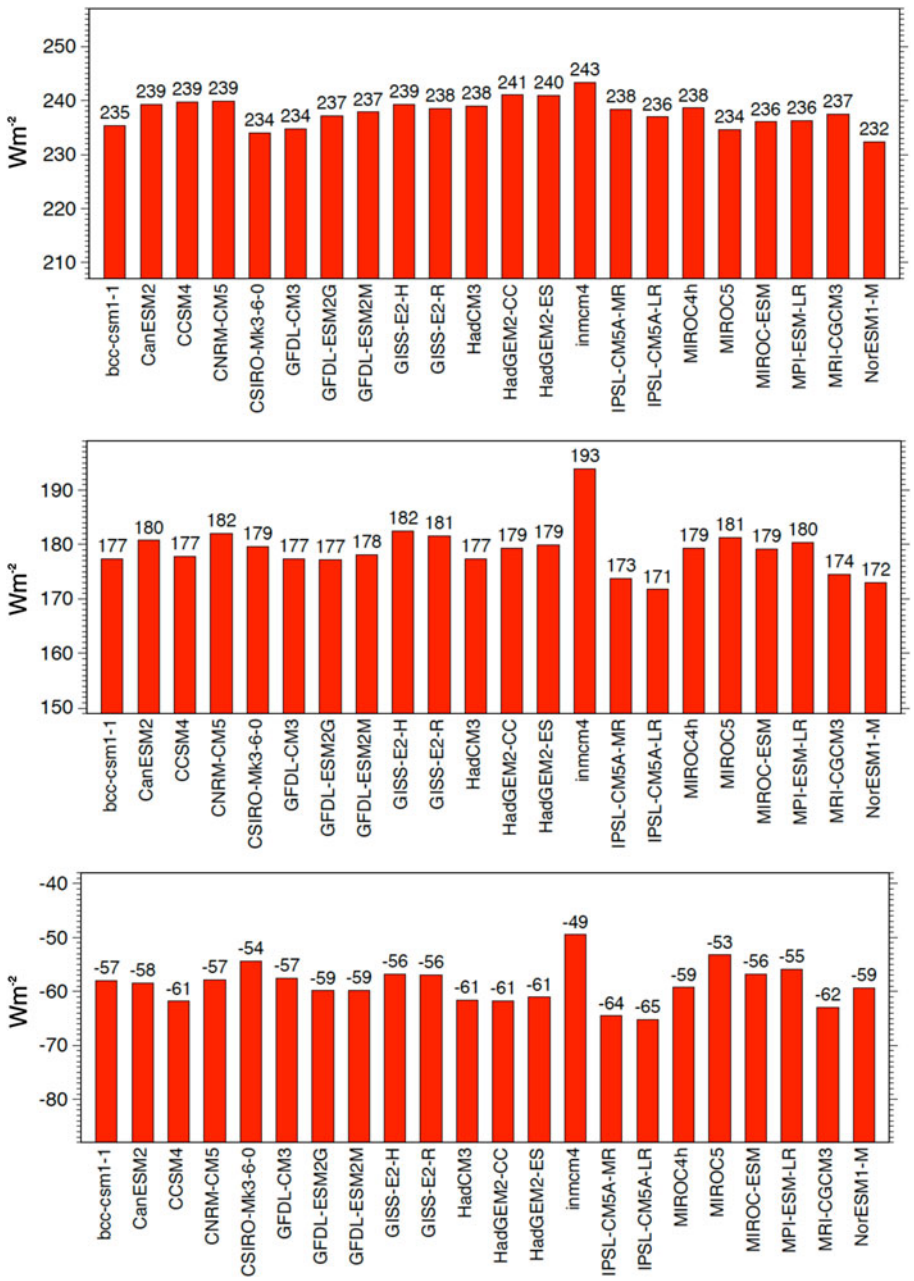

Fig. 4 Global annual mean thermal radiation budgets calculated by 22 CMIP5/IPCC AR5 models for present day climate. Net thermal radiation at the surface (*lowermost panel*), within the atmosphere (*middle panel*), and emitted to space (*uppermost panel*). Units Wm^{-2}

overestimations in the newer CMIP5 models. Some of the newer models show reduced biases, but others show the opposite. As potential causes for this overestimation a lack of water vapor as well as aerosol absorption in many of the GCMs has been put forward (e.g., Wild et al. 2006), while some studies also argue that cloud absorption has been underestimated in the GCMs (see Wild (2008) for a review of these issues). Here we document that also the latest model generation used in the 5th IPCC assessment report still shows a tendency towards excessive insolation at the Earth's surface.

In contrast, the surface solar fluxes calculated in the ERA40 reanalysis (cf. Sect. 3) are on average lower than the observational references (Fig. 11, left). Compared to the 760 GEBA sites, the average underestimation is -6 Wm^{-2} sites (-4.7 Wm^{-2} with additional latitudinal weighing). With a global mean of 179 Wm^{-2}, the downward surface solar radiation in ERA40 is, however, substantially lower than in any of the CMIP5 models shown in Fig. 5. This underestimation might be related to problems in the representation of clouds and particularly cloud radiative properties in ERA40 as pointed out by Allan et al. (2004), Uppala et al. (2005), Trenberth and Fasullo (2010), and Berrisford et al. (2011).

To obtain a best estimate for the globally averaged downward solar radiation, the associated biases of the individual models and ERA40 are related to their

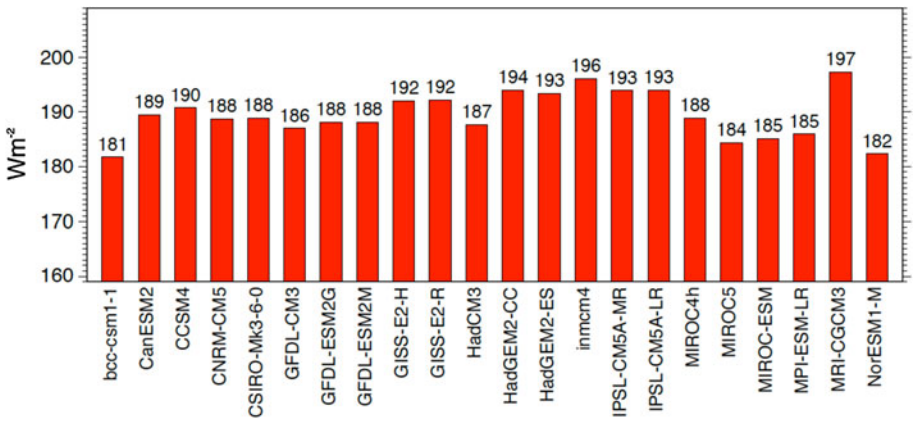

Fig. 5 Global annual mean downward solar radiation at Earth's surface under present day climate calculated by 22 CMIP5/IPCC AR5 models as listed in Table 2. Units Wm^{-2}

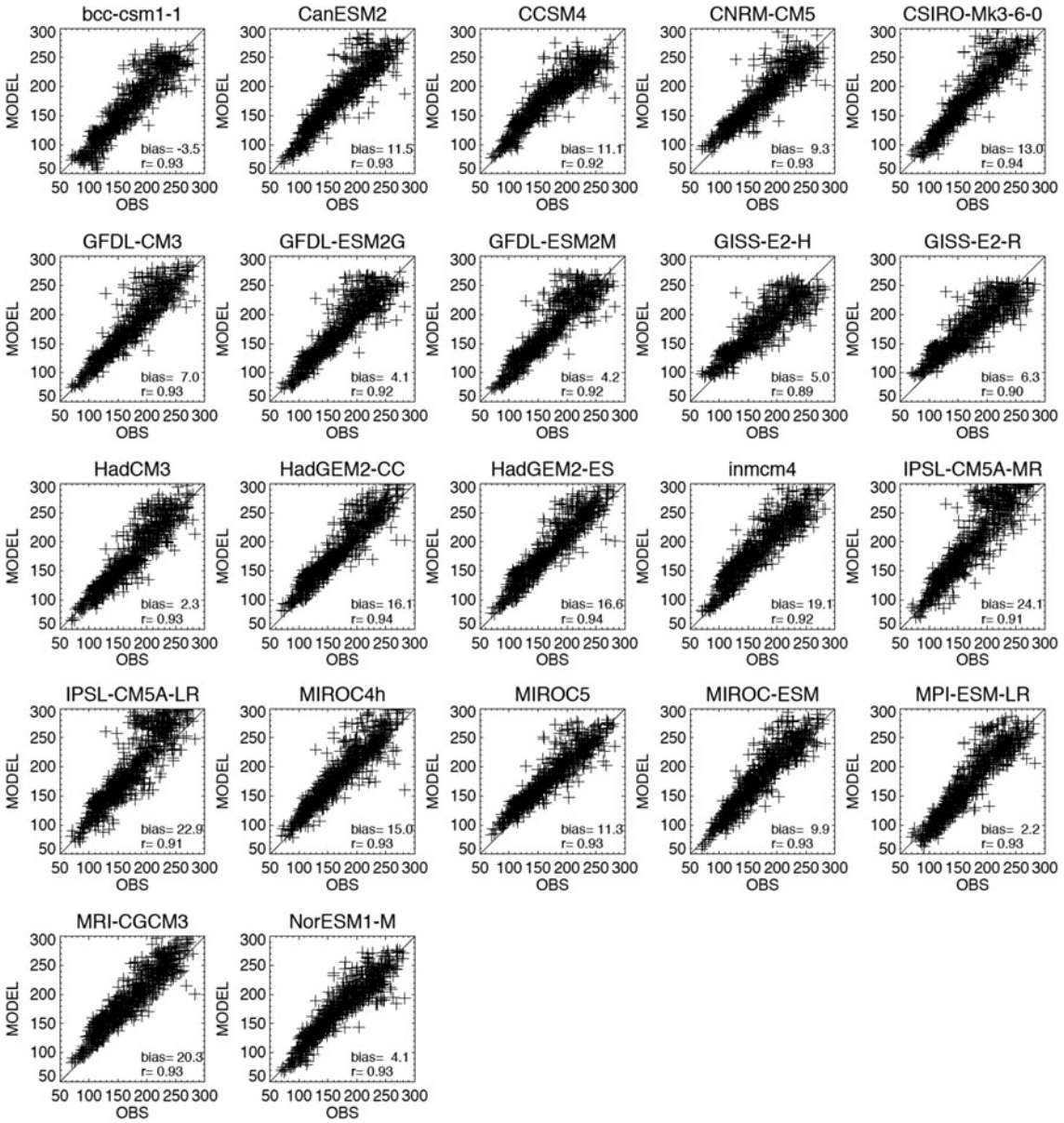

Fig. 6 Comparison of long-term annual mean downward solar radiation at Earth's surface observed at 760 sites from GEBA and calculated by 22 CMIP5/IPCC AR5 models as listed in Table 2. Units Wm^{-2}

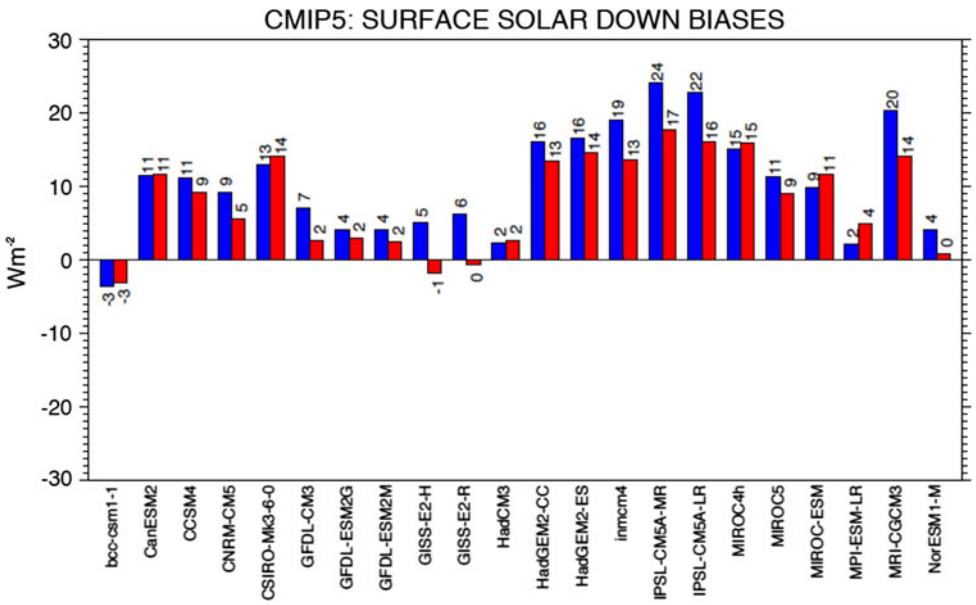

Fig. 7 Average bias (model–observations) in downward solar radiation at Earth's surface calculated in 22 CMIP5 models at 760 sites from GEBA (in *blue*) and at 42 sites from BSRN (in *red*). Units Wm^{-2}

respective global mean values for the downward solar radiation in Fig. 12. In this Figure, each cross represents a climate model, with its mean bias in downward solar radiation compared to the 760 surface sites from GEBA on the horizontal axis (as given in Figs. 6, 7), and its respective global mean value on the vertical axis (as given in Fig. 5). A clear tendency can be seen that models, which show a stronger overestimation of insolation at the surface sites, also tend to have a higher global mean insolation. The model-calculated downward solar radiation biases averaged over the 760 GEBA sites in the various models show a good correlation with their respective global mean values (correlation coefficient 0.80). The linear regression displayed in Fig. 12 between the model biases and their respective global means is significant at the 95 % level. A best estimate for the global mean downward solar radiation can be inferred from the linear regression at the intersect where the bias against the surface observations becomes zero (indicated by the dashed lines in Fig. 12). This way, a best estimate for the globally averaged downward solar radiation at Earth's surface of 184.6 (±1.0) Wm^{-2} is obtained. The uncertainty in the parentheses is given by the standard error of the linear fit in Fig. 12 that determines the uncertainty of the vertical axis intersect at the zero bias line.

In order to test the robustness of this estimate for the global mean downward solar radiation, we repeated the same analysis, but this time considering the area-weighed latitudinal distribution in the calculation of the model biases (based on Fig. 8) instead of the simple averaging over the station biases as used in Fig. 12. The same linear regression yielded a very similar best estimate of 184.3 (±1.0) Wm^{-2}. Therefore the global mean estimate seems to be fairly insensitive with respect to the way the model biases at the 760 sites are aggregated. We further repeated the same analysis, but now based on model biases determined at the 42 and 38 BSRN sites with pyranometer and diffuse/direct measurements, respectively, instead of the 760 GEBA sites. With the model biases determined as average over the pyranometer records available at the 42 BSRN sites, a best estimate of 185.9 (±1.2) Wm^{-2} is obtained for the global mean downward solar radiation. Similarly, a best estimate of 186.1 (±1.2) Wm^{-2} is obtained when the biases are determined using the direct plus diffuse radiation records available at 38 BSRN sites.

In summation, despite differences in the geographical distribution and density of the networks used here, as well as different measurement techniques employed, the resulting global mean estimates differ by less than 2 Wm^{-2}. Thus, the best estimate obtained in this regression analysis seems rather robust with respect to the exact specification and extension of the observational reference network. This analysis therefore supports a best estimate for the global mean downward solar radiation constrained by surface observations near 185 Wm^{-2}.

4.2.2 *Thermal radiation*

The thermal radiation is of central importance in the discussion of climate change, as it is most directly influenced by changes in the concentration of radiatively active gases in the atmosphere. In the CMIP5 GCMs, the net thermal budgets at the surface and in the atmosphere show larger discrepancies than at the TOA, as can be inferred from Fig. 4 and Table 3. This is again a consequence of the lack of unambiguous reference values to constrain the simulated

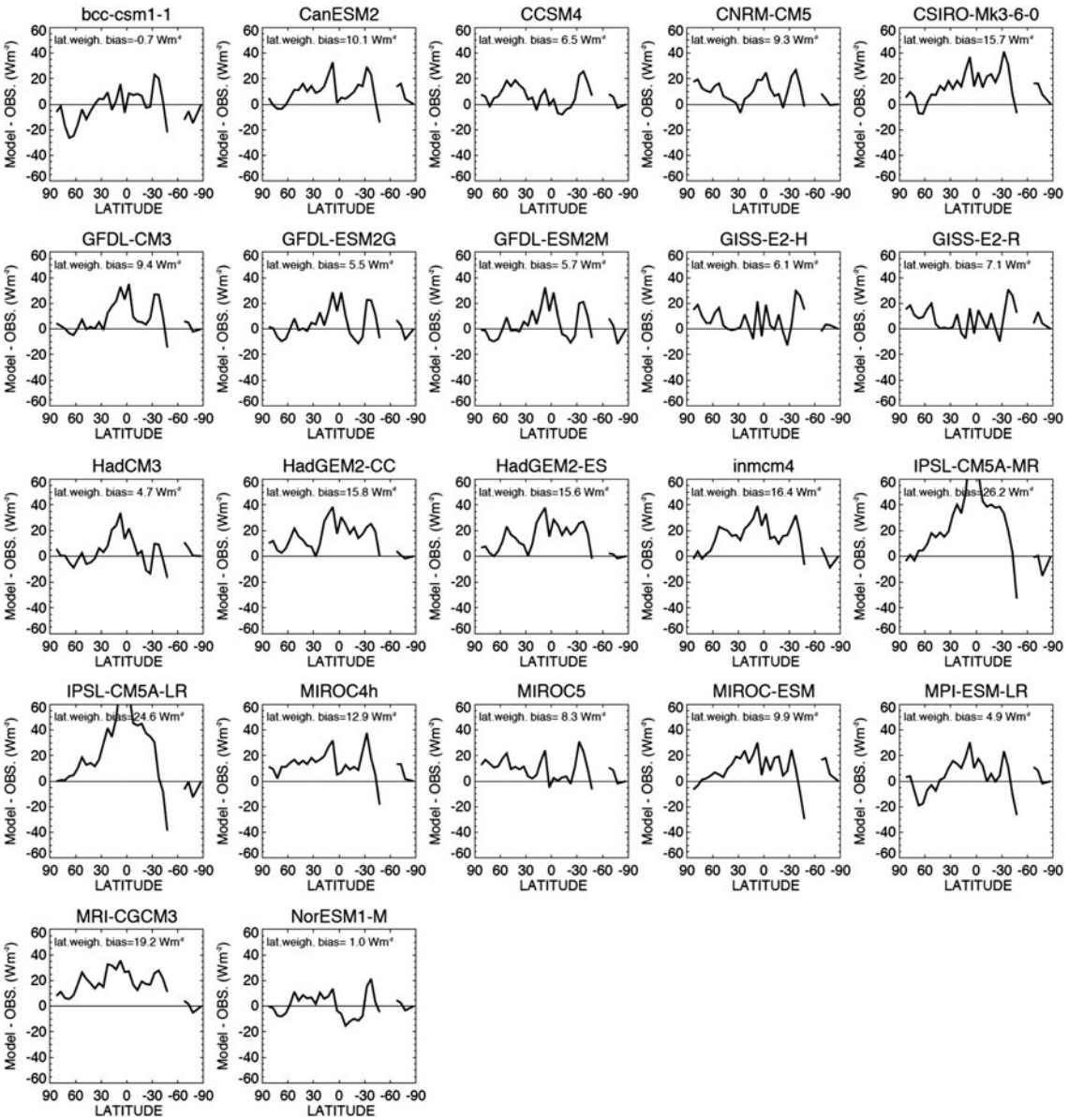

Fig. 8 Downward solar radiation biases at 760 observation sites as function of latitude, for 22 different CMIP5 models as listed in Table 2. Biases averaged over sites within 5° latitudinal bands. Surface observations from GEBA. Units Wm^{-2}

surface and atmospheric thermal budgets, while the TOA fluxes are typically tuned on a global mean basis against satellite reference values (see Sect. 4.1).

The surface thermal budget consists of the downward and upward flux components. From a modeling point of view, the upward flux can be determined straightforward using the surface temperature and the Stefan–Boltzman law, and is therefore affected with less uncertainty. Modeling of the downward thermal flux is more challenging, as it depends on the complex vertical structure of the physical properties of the atmosphere. It is also the flux that most immediately responds to alterations in the concentration of radiatively-active gases in the atmosphere and therefore can be seen as an indicator of the atmospheric greenhouse effect as experienced at the surface. Global mean downward thermal radiation estimates as calculated by the 22 CMIP5 GCMs are shown in Fig. 13. The multimodel mean downward thermal radiation amounts to 338 Wm^{-2}. A substantial spread is seen in Fig. 13, with a range of 20 Wm^{-2} and a standard deviation of 4.8 Wm^{-2}, marking the highest standard deviation of all energy balance components considered in Table 3. To better constrain this considerable range, we use all available information contained in the surface observational records of downward thermal radiation. Downward thermal radiation measurements have historically been performed at far fewer sites

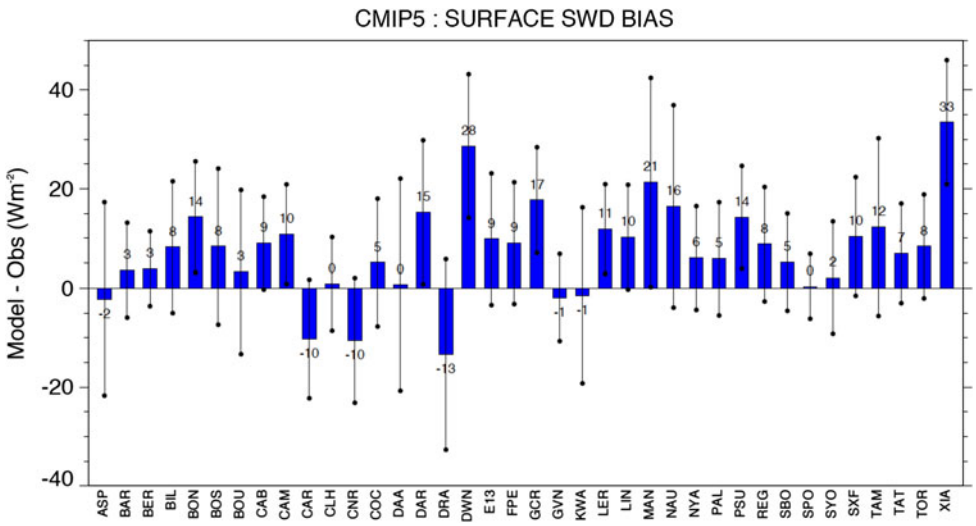

Fig. 9 Multimodel mean bias in downward solar radiation at Earth's surface (model–observations) at 38 different BSRN sites. The distribution of individual model biases is further indicated with a vertical line covering ± one standard deviation. Station abbreviations explained in Table 1. Units Wm^{-2}

than downward solar radiation measurements, since it requires a more sophisticated measurement technology (Ohmura et al. 1998). It is only with the initiation of BSRN, which specifies downward thermal radiation as a mandatory measurement in its guidelines, that such measurements are gradually starting to become available on a widespread basis. In addition, a small number of downward thermal radiation records are also available from GEBA, typically at lower quality (Wild et al. 2001). With the expansion of the BSRN network, the number of stations with downward thermal radiation measurements has recently been growing substantially. Here we use the latest status of the BSRN archive as available in June 2012 to allow the inclusion of an unprecedented wealth of observations of downward thermal radiation. We were able to establish downward thermal radiation climatologies from multiyear records at 41 BSRN stations (Table 2). Again, the gridded model fields were interpolated to the measurement sites using the four surrounding grid points, weighted by their inverse spherical distance. In addition, a correction has been applied whenever the elevation of the observation sites and the corresponding model grid points differ significantly, since downward thermal radiation, unlike solar radiation, shows a strong and systematic dependency on altitude (Wild et al. 1995a). Where substantial height differences between model and real topography exist, a height correction of 2.8 Wm^{-2} per 100 m was therefore applied (Wild et al. 1995a).

Since no information on orography was available from the inmcm4 model in the CMIP5 data archives, we do not include this particular model in the thermal flux analysis, leaving 21 CMIP5 models for the assessment. Figure 14 compares long-term annual mean values of downward thermal radiation at the 41 sites as calculated by each individual model and as observed. Overall the agreement seems excellent, as also indicated in the high correlation coefficients of at least 0.98. They are again partly a result of the common latitudinal dependence of both modeled and observed fluxes. Linear regression slopes are further indicated as dashed lines in Fig. 14. They generally are very close to one, and the average over all slopes matches exactly 1.00. This indicates that the model biases do not seem to depend systematically on the absolute magnitudes of the fluxes.

A closer inspection reveals, however, that the models show systematic mean biases. This mean bias is generally negative, as illustrated also in Fig. 15. 18 out of the 21 models systematically underestimate on average the fluxes at the BSRN sites [Figs. 14, 15 (red bars)]. The multimodel mean underestimation amounts to -6.0 Wm^{-2}, with a median underestimation of -6.1 Wm^{-2}. If the above-mentioned corrections for the altitudinal differences between observation sites and associated model grid points are omitted, the differences between models and observations are enhanced by 1.5 Wm^{-2} on average, suggesting that the stations are, on average, located slightly lower than the related model grid points.

The ERA40 shows a fairly good agreement in their calculated downward thermal fluxes with the 41 BSRN records, with only a slight underestimation of 2.5 Wm^{-2} (Fig. 11, right).

To investigate the robustness of the model biases, and for comparison with earlier studies, we repeated the evaluation of the downward thermal radiation with a somewhat different observational dataset that has been used in previous assessments (Wild et al. 2001; Wild 2008). This dataset consists of 26 sites from GEBA and 19 sites from BSRN that were available at the time, geographically distributed as shown in Wild et al. (2001). Using this dataset, and considering the 21 CMIP5 models, a mean and median underestimation of -7.1 and -6.1 Wm^{-2}, is found, thus similar in magnitude despite

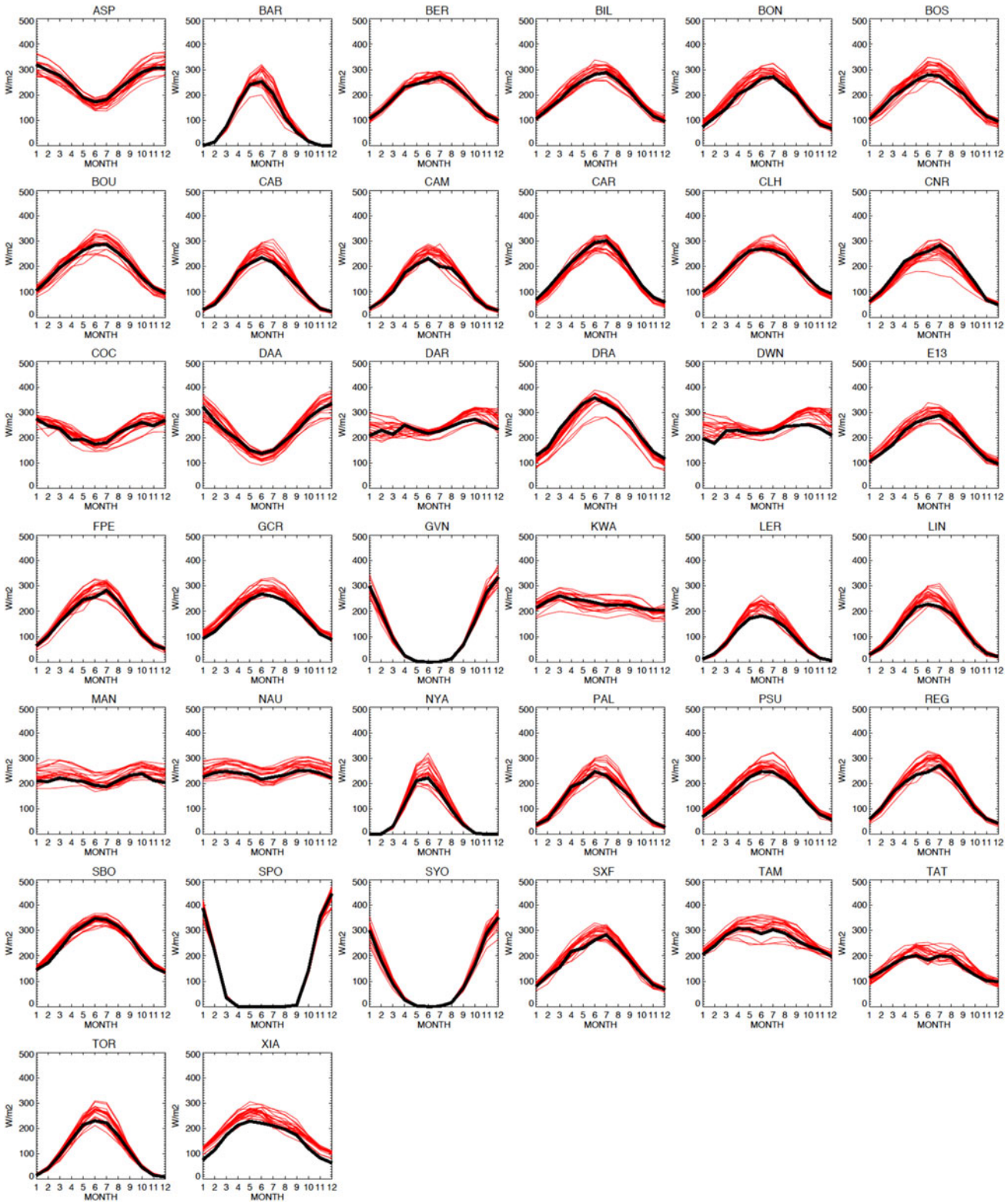

Fig. 10 Mean annual cycles of downward solar radiation at Earth's surface as observed at 38 BSRN sites (*thick black lines*) and calculated by 22 CMIP5 models (*thin red lines*). Observations determined as sum of diffuse and direct radiation measurements. For explanation of abbreviated station names and station coordinates see Table 1. Units Wm^{-2}

Table 4 Comparison of surface radiative flux biases in successive model versions of institutions participating in both CMIP3 and CMIP5 projects

	Downward solar radiation (against 760 GEBA sites)		Downward thermal radiation (against 45 BSRN/GEBA sites)	
CMIP3/CMIP5 model version	CMIP3	CMIP5	CMIP3	CMIP5
GFDL CM2/CM3	−2.4	7.0	−10.4	−3.2
CNRM CM3/CM5	−12.7	9.3	−1.9	−13.2
GISS EH/E2H	6.8	5.0	n.a.	−2.2
GISS ER/E2R	5.9	6.3	n.a.	−6.1
INM CM3/CM4	9.3	19.1	−0.4	n.a.
MIROC HR/MIROC5	14.2	11.3	−9.0	−1.5
MPI ECHAM5/ESM LR	−10.6	2.2	−0.4	−0.6
MRI CGCM2/CGCM3	20.1	20.3	−10.8	−15.5
NCAR CCSM3/CCSM4	0.8	11.1	−6.9	−9.6
UKMO HadCM3/HadGEM2-ES	0.1	16.6	−10.2	−7.4

Biases in Wm^{-2} (model–observations) averaged over 760 GEBA sites for the downward solar and over 45 GEBA/BSRN sites for the thermal radiation. CMIP3 results reproduced from Wild (2008)

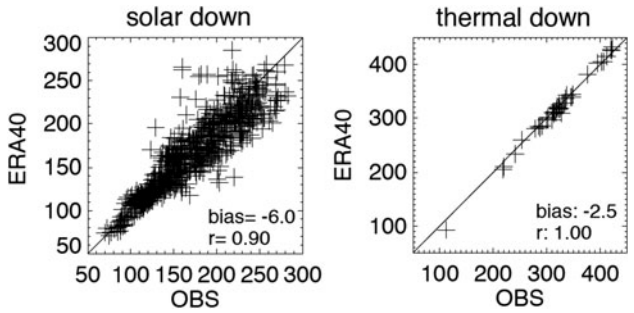

Fig. 11 Comparison of long term annual mean surface fluxes calculated by the ERA40 re-analysis against observations of downward solar radiation at 760 sites from GEBA (*left*), and of downward thermal radiation at 41 sites from BSRN (*right*). Units Wm^{-2}

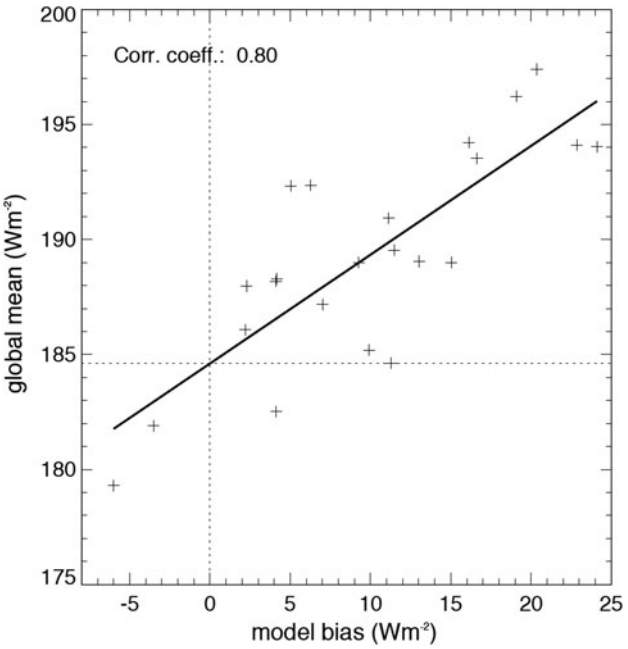

Fig. 12 Global mean surface downward solar radiation of 22 CMIP5/IPCC AR5 models and ERA40 versus their respective biases averaged over 760 surface observation sites from GEBA. A "best estimate" for the global mean downward solar radiation of 184.6 Wm^{-2} is inferred at the intersect between the linear regression line and the zero bias line (*dotted lines*). Units Wm^{-2}

the substantially differing underlying observational dataset. All models show a negative bias in their thermal radiation compared to these 45 sites (Fig. 15, blue bars). As with the shortwave analyses in Sect. 4.2.1, the results seem rather insensitive to the exact choice of the surface reference stations. The model biases determined here are of similar magnitude as in earlier model generations [-5.6 Wm^{-2} in the CMIP3 model, -8 Wm^{-2} in the AMIPII models (Wild 2008)]. Specifically, in Table 4, the downward thermal radiation biases of successive model versions that took part in CMIP3 and CMIP5 are compared, based on averaging the model biases at the 26 GEBA and 19 BSRN sites as used in Wild et al. (2001) and Wild (2008). Similarly to the downward solar radiation before, there is no clear evidence for reduced biases in the newer CMIP5 model versions.

As in earlier assessments, the magnitude of the overall downward thermal radiation biases in the CMIP5 models seems to be similar, but of opposite sign to the respective biases in the surface solar radiation. This reflects the overall error balance between excessive absorbed solar and lack of downward thermal radiation at Earth's surface typically found in climate models.

Annual multimodel mean downward thermal radiation biases at the 41 individual BSRN sites are shown in Fig. 16. One standard deviation of the individual CMIP5

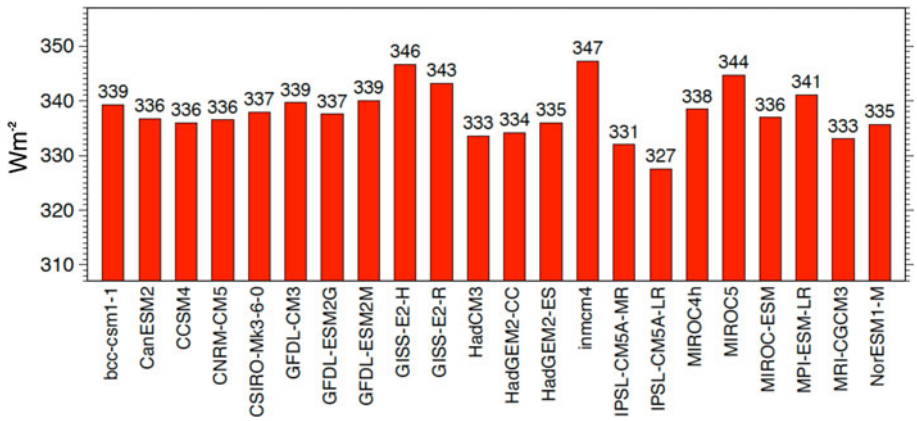

Fig. 13 Global annual mean downward thermal radiation at Earth's surface under present day climate calculated by 22 CMIP5/IPCC AR5 models as listed in Table 2. Units Wm^{-2}

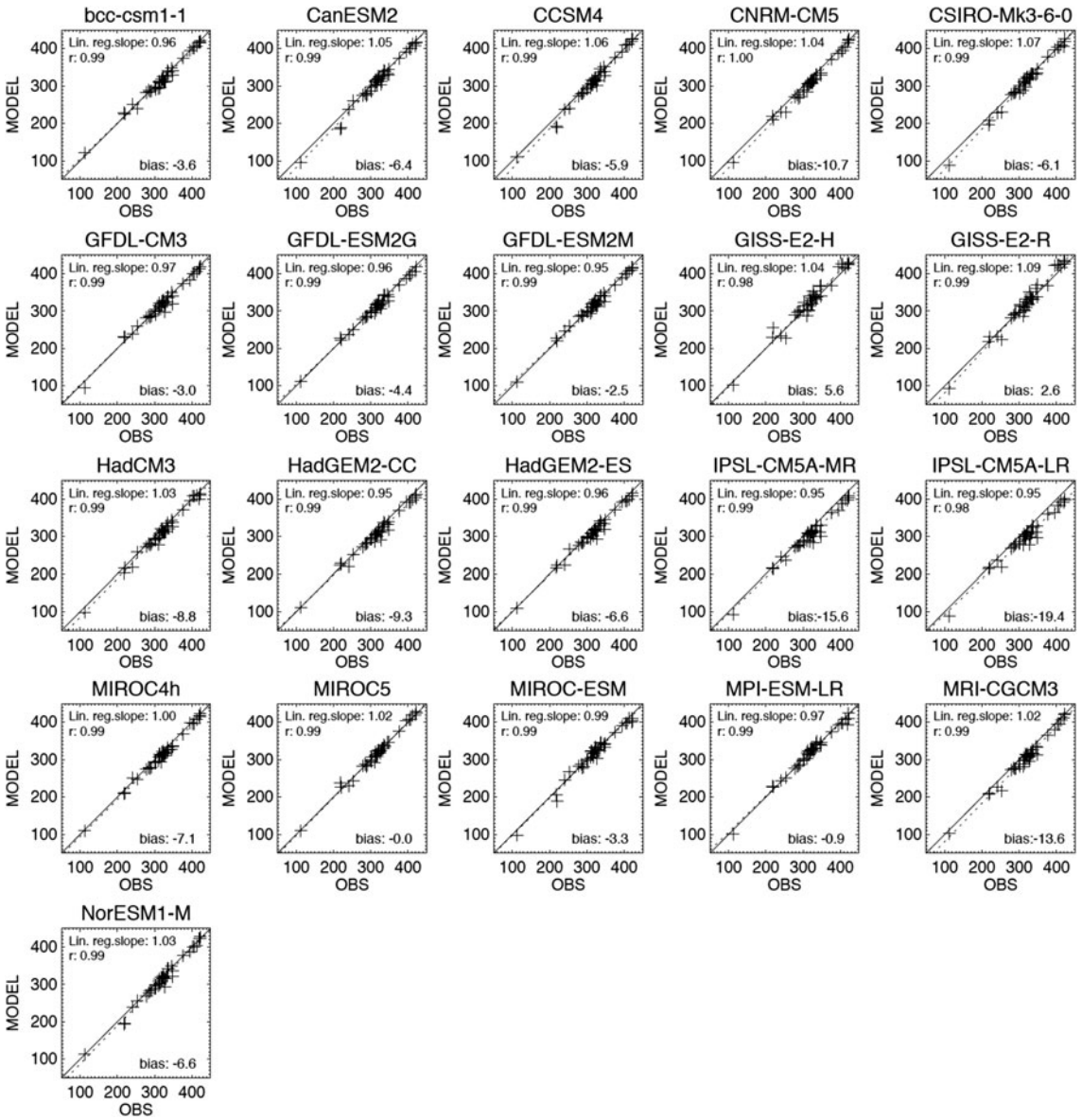

Fig. 14 Comparison of long-term annual mean downward thermal radiation observed at 41 sites from BSRN and calculated at these sites by 21 CMIP5/IPCC AR5 models. Units Wm^{-2}

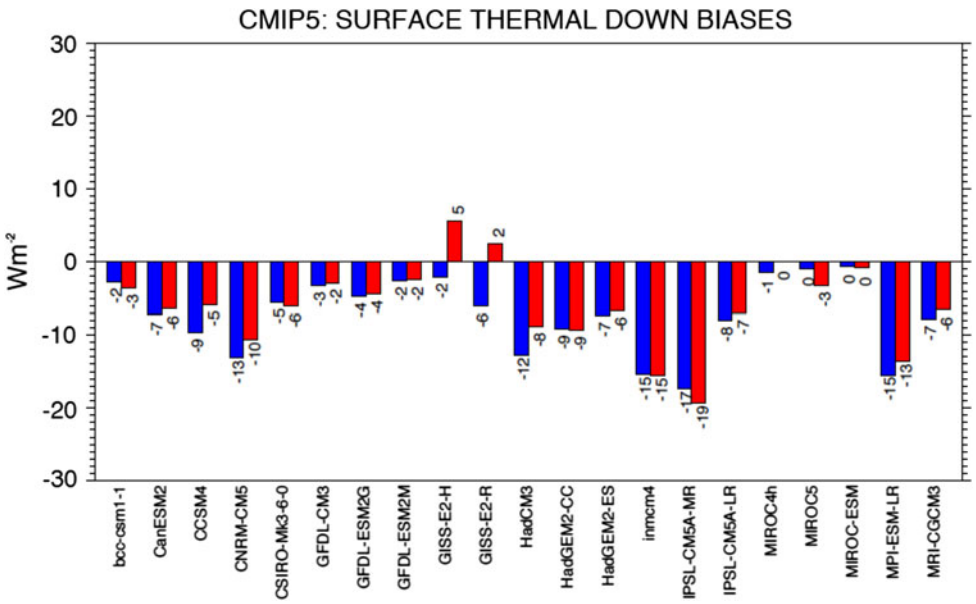

Fig. 15 Average bias (model–observations) in downward thermal radiation at Earth's surface calculated in 21 CMIP5 models at 41 sites from BSRN (in *red*), and at 45 sites from an earlier dataset based on 26 GEBA/19 BSRN sites (in *blue*). Units Wm^{-2}

model biases is further indicated. The multimodel mean downward thermal radiation is underestimated at 39 out of 41 sites. Again there is also no evidence that biases at the ocean BSRN stations located on small islands are systematically different from those over land.

Annual cycles of downward thermal radiation as observed at the 41 BSRN sites and simulated by the CMIP5 models are shown in Fig. 17. The observed annual cycle is again shown in black, the annual cycles simulated by the various models in red. At many of the sites the observed annual cycles are at the upper or at least towards the upper bound of the various model estimates, in line with the evidence from the annual mean biases in Fig. 16. The month with maximum downward thermal radiation (peak summer month) is in the models on average 5.5 Wm^{-2} lower than observed, while the month with minimum downward thermal radiation (peak winter month) is at 6.0 Wm^{-2} slightly more underestimated. Overall this suggests that the underestimation of downward thermal radiation on average in the models does not greatly vary with season in absolute terms.

The underestimation of the downward thermal radiation is also a known long standing problem in many GCMs. Evidence that global mean downward thermal radiation should be higher than typically simulated in climate models has been presented in earlier studies (Wild et al. 1995b; Garratt and Prata 1996; Wild et al. 1998; Wild et al. 2001; Markovic et al. 2008; Bodas-Salcedo et al. 2008; Wild 2008), and is confirmed here using the latest and most comprehensive dataset of direct observations as well as the latest generation of global climate models. It was also shown in earlier studies that radiation models tend to underestimate the thermal emission of the cloud-free atmosphere (e.g., Dutton 1993; Chevallier and Morcrette 2000; Wild et al. 2001; Markovic et al. 2008). The semi-empirical formulations of the water vapor continuum are considered as a major source of uncertainty in the thermal flux calculations (Wild et al. 2001; Iacono et al. 2000).

To obtain a best estimate for the global mean downward thermal radiation in the same way as before for the downward solar radiation, we again relate the model and ERA40 biases to their respective global mean values. Figure 18 shows the model simulated global means in downward thermal radiation (as given in Fig. 13) as function of their biases averaged over the 41 BSRN sites (as given in Figs. 14, 15, red bars). A very distinct relationship can be noted between the model biases and their global mean values, with a correlation of 0.94 (Fig. 18). There is a clear tendency that the more a model underestimates the downward thermal radiation at the BSRN sites, the lower is also its global mean value. The associated linear regression is therefore highly significant. The zero model bias corresponds to a global mean downward thermal radiation of 342.3 Wm^{-2}, as indicated by the dashed lines in Fig. 18, which is considered as best estimate in this framework. This value is determined from the linear regression with a standard error of ± 0.5 Wm^{-2}. The same analysis with the older dataset with the 45 GEBA/BSRN sites yields a very similar relationship, with a best estimate of 342.8 ± 0.8 Wm^{-2}. Again the best estimate derived in this way is not very sensitive to the detailed specifications of the surface observations. This robustness may be favored by the lack of systematic dependencies of the model biases on geographical locations and seasons, which may improve the representativeness of the networks with limited numbers of sites.

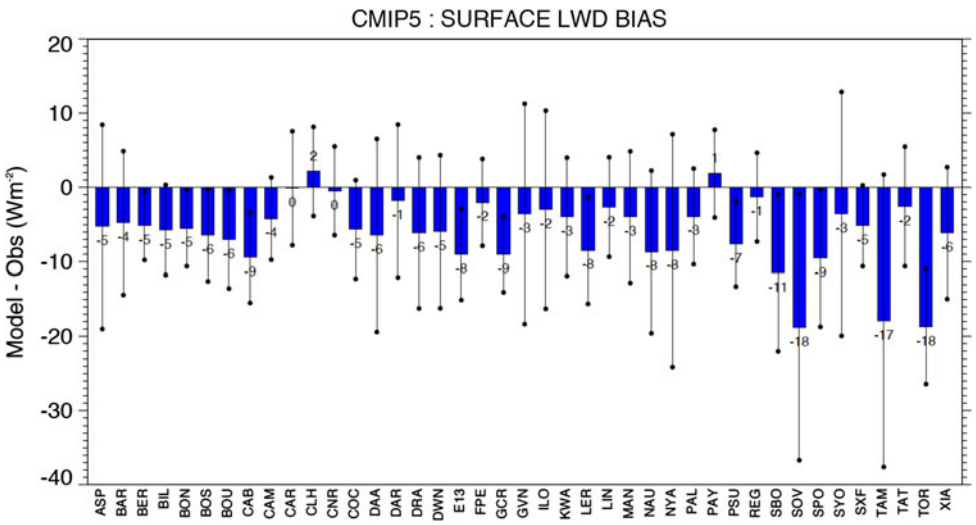

Fig. 16 Multimodel mean biases (model–observations) in downward thermal radiation at 41 different BSRN sites. The distribution of individual model biases is further indicated with a vertical line covering ± one standard deviation. Station abbreviations explained in Table 1. Units Wm^{-2}

The estimates derived here are also close to the best estimates obtained in our earlier studies based on comparisons of older and fewer models with fewer observations (344 Wm^{-2}, Wild et al. (2001); 345 Wm^{-2}, Wild et al. (1998)).

5 Discussion of Earth's global mean energy balance

Along with an evaluation of the radiation budgets in the latest generation of global climate models, the above analysis aimed at providing best estimates for the global mean surface radiative fluxes, using direct surface observations as constraints. These estimates are incorporated into a new global energy balance diagram in Fig. 1, along with recent best estimates for the other energy balance components, and are discussed in the following. In addition, we made an attempt to attribute uncertainty ranges to the major components in Fig. 1. Such uncertainty information is lacking in most of the published global energy balance diagrams. Figure 1 is representative for conditions at the beginning of the twenty first century, since the BSRN surface radiation climatologies reflect this period, and the CERES EBAF estimates used here for the TOA fluxes cover the first decade of the new millennium (Sect. 2).

5.1 TOA fluxes

Following the discussion in Sect. 4.1, in Fig. 1 we use for the global mean TOA components representative for the beginning of the 21th century the recent estimate of 340 Wm^{-2} for the solar irradiance based on SORCE, with a rounded uncertainty range from 340 to 341 Wm^{-2} (Kopp and Lean 2011), for the reflected solar radiation the estimate from CERES EBAF of 100 Wm^{-2} (2-sigma uncertainty range from 96 to 100 Wm^{-2}) (Loeb et al. 2009), and for the outgoing thermal radiation the CERES EBAF estimate of 239 Wm^{-2} (2-sigma uncertainty range from 236 to 242 Wm^{-2}) (Loeb et al. 2009). The difference between the net absorbed solar radiation, which amounts to 240 Wm^{-2}, and the 239 Wm^{-2} outgoing thermal radiation takes into account in a rounded way the effect of the approx. 0.6 Wm^{-2} global energy imbalance inferred from ocean heat content measurements (see discussion in Sect. 4.1). The absorbed solar and outgoing thermal TOA fluxes are about 5 Wm^{-2} larger than some of the earlier publications of global energy balance estimates (e.g., Kiehl and Trenberth 1997), which were adjusted from the global mean outgoing thermal radiation, determined at 235 Wm^{-2} during the Earth Radiation Budget Experiment (ERBE, Barkstrom 1984) that took place over the period 1985–1989.

5.2 Surface solar fluxes

With respect to the solar fluxes at Earth's surface, we inferred in this study a global mean value near 185 Wm^{-2} for the downward solar radiation, which fits best to the direct surface observations (Sect. 4.2.1). We attribute to this value an uncertainty range from 179 to 189 Wm^{-2} (Fig. 1), which we justify as follows. The upper bound of this range is given by the multimodel mean of the CMIP5 models. A conservative conclusion of the analyses in Sect. 4.2.1 is that, at the very least, there is no evidence that the models overall underestimate the downward solar radiation. Any value higher than the multimodel mean of these models, at 189 Wm^{-2} (Table 3), seems therefore difficult to justify. On the other hand, a simple subtraction of the average model bias at 760 GEBA stations (10.5 Wm^{-2}) from the model-calculated global mean values would result in a value of 179 Wm^{-2}. This is a conservative estimate at the low end, as some of the GEBA measurements might be biased low due to

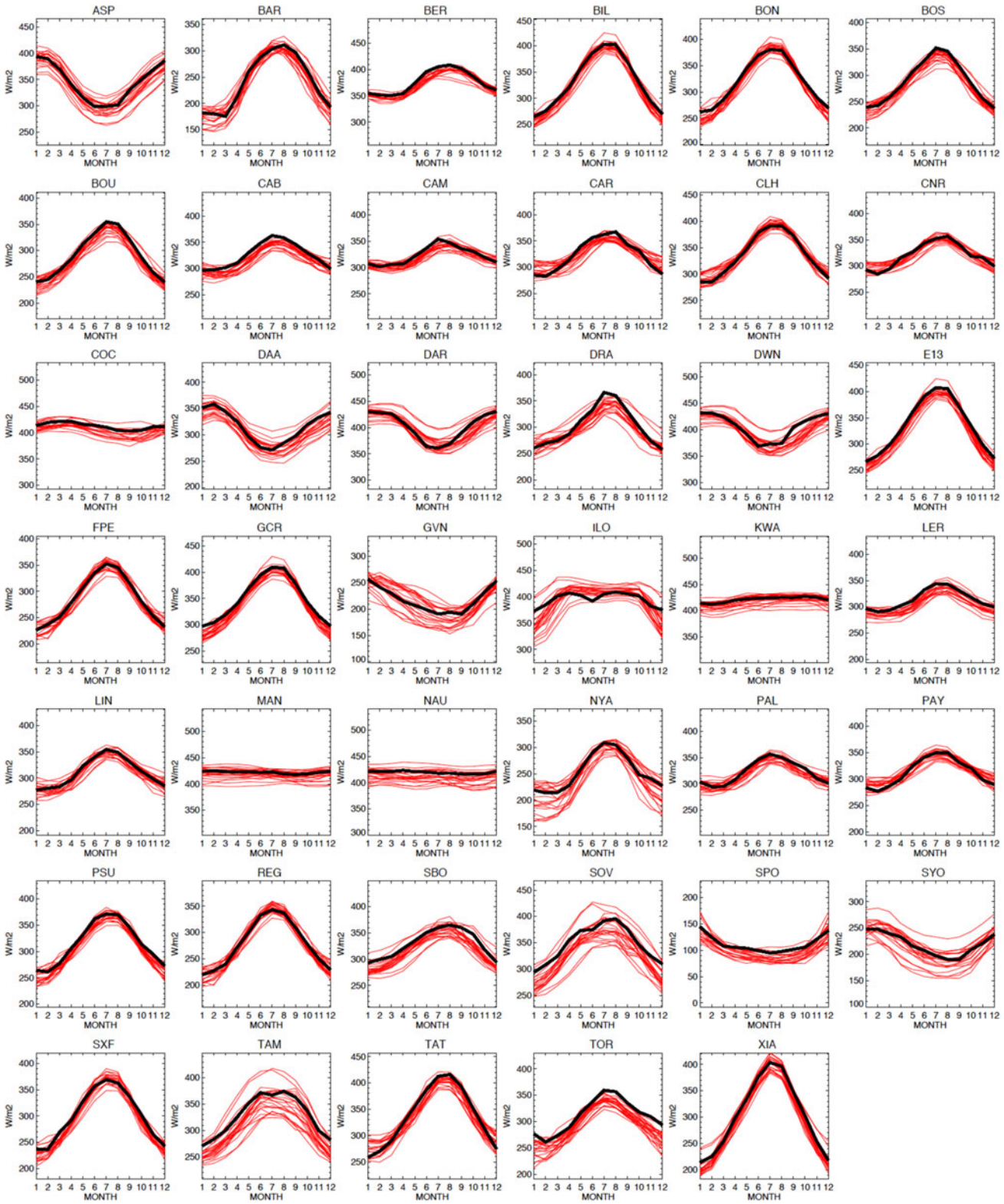

Fig. 17 Mean annual cycles of downward thermal radiation as observed at 41 BSRN sites (*thick black lines*) and calculated by 21 CMIP5 models (*thin red lines*). For explanation of abbreviated station names and station coordinates see Table 1. Units Wm^{-2}

urbanization effects not resolved in the GCMs. This may also explain a part of the somewhat stronger biases found at the GEBA sites compared to the BSRN sites, which are predominantly situated in non-urban environments. The lower bound of this uncertainty range is further corroborated by the analysis of the downward solar radiation fields

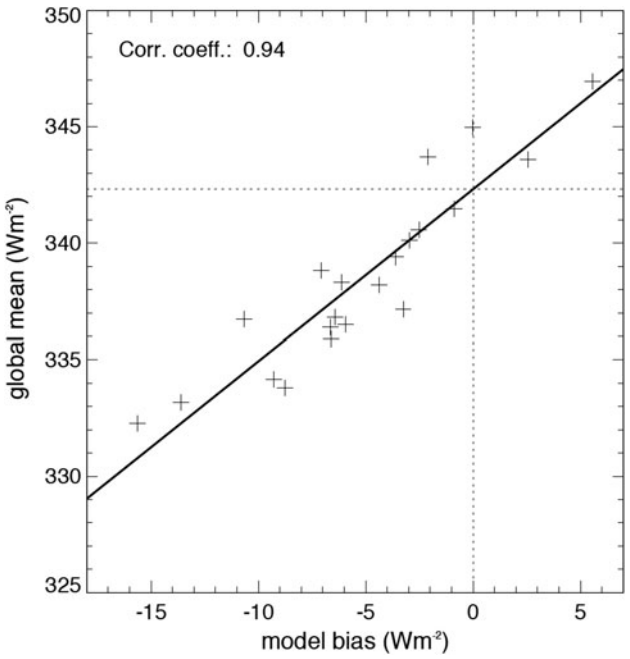

Fig. 18 Global mean downward thermal radiation of 21 CMIP5/IPCC AR5 models and ERA40 versus their respective mean biases averaged over 41 surface observation sites from BSRN. A "best estimate" for the global mean downward thermal radiation of 342.3 Wm^{-2} is inferred at the intersect between the linear regression line and the zero bias line. Units Wm^{-2}

calculated in ERA40 (cf. Sect. 4.2.1). This reanalysis determines a global mean value of 179 Wm^{-2} and thus marks the low end of the uncertainty range. Comparisons of the downward solar radiation of ERA40 with the 760 sites from GEBA show an underestimation of -6 Wm^{-2}averaged over all sites (cf. Figure 11, left). This suggests that there is at least no indication that the ERA40-calculated global mean downward shortwave radiation of 179 Wm^{-2} should be too high. A simple bias correction of the ERA40 estimate, by adjusting the global mean by its overall bias (-6 Wm^{-2}), would give 185 Wm^{-2}, matching the best estimate proposed here.

The different published estimates that infer the downward solar radiation from satellite retrievals show an even larger spread in their global means than the CMIP5 models in Fig. 5. Depending on the product, they range from 172 to 192 Wm^{-2} (Zhang et al. 2004; Kato et al. 2011; Hatzianastassiou et al. 2005; Gupta et al. 1999), which may indicate a higher uncertainty range than given in Fig. 1. Yet validations of these satellite-derived products against different versions of surface reference datasets from GEBA and BSRN published in the literature suggest that the products with low global mean values of downward solar radiation tend to have a negative mean bias against the surface observations, while the products with global means at the high end show positive biases. Specifically, Hatzianastassiou et al. (2005), who determine a global mean value of 172 Wm^{-2}, report negative biases compared to the GEBA and BSRN sites, of -6.5 and -14 Wm^{-2} on average, respectively. On the other hand, Kato et al. (2012) and Zhang et al. (2004), whose estimates of 192 and 189 Wm^{-2} are at the high end, report positive mean biases of $+3.8$ and $+2.0$ Wm^{-2} against BSRN data, respectively. Simple adjustments of the different satellite-derived estimates by subtracting the respective biases from their global means brings these estimates into better agreement and within the uncertainty limits given in Fig. 1. A similar regression as done in Sect. 4.2.1 with the GCM global means versus their biases, but now instead with the abovementioned global means of the satellite-derived products versus their biases compared GEBA and BSRN as published in the cited papers (not necessarily based on identical sets of surface observations), supports a similar best estimate as previously obtained in Fig. 12 with the GCMs. In their latest assessment, Kato et al. (in press) revised their abovementioned global mean downward solar radiation value of 192 Wm^{-2} (Kato et al. 2012) down to 187 Wm^{-2} (Surface EBAF version Ed2.6r covering the period March 2000 through Feb. 2010), thus very close to our best estimate obtained here. A better treatment of a diurnal cycle in adjusting surface solar irradiance significantly reduced their surface solar radiation estimate (Kato et al. in press). Thus, these latest satellite-derived estimates of the global mean downward solar radiation converge with our estimate derived here to within 2 Wm^{-2}. This consistency is achieved with completely independent approaches, which adds confidence to the estimate portrayed here.

An estimate of the reflected solar radiation at Earth's surface is obtained in Fig. 1 considering in addition to the downward solar radiation the surface albedo. Assuming a global mean surface albedo of 0.13, from the best estimate of 185 Wm^{-2} solar energy incident at the Earth's surface, 24 Wm^{-2} are reflected. The value of 0.13 corresponds to the multimodel mean albedo of the CMIP5 models used here. It is similar to the surface albedo values used in previous studies of the surface energy balance (e.g., Trenberth et al. 2009) and also close to the estimates in the reanalyses from the European Center for Medium Range Weather Prediction, ERA Interim (0.127) and ERA 40 (0.125) (Berrisford et al. 2011). With 24 Wm^{-2} reflected out of the total of 185 Wm^{-2} of downward solar radiation, this leaves an amount of 161 Wm^{-2} absorbed at the Earth's surface (Fig. 1). Translating the above defined uncertainty range of the downward solar radiation (179–189 Wm^{-2}) into absorbed solar radiation assuming the same surface albedo of 0.13, results in a range of 156–164 Wm^{-2}. Uncertainties in the global mean surface albedo, taken here as ± 0.01 (covering most of the published global mean albedo estimates), may expand the uncertainty range on the order of 4 Wm^{-2}. Thus, an uncertainty range of 154–166 Wm^{-2} is

adopted for the absorbed surface solar radiation in Fig. 1, as well as a corresponding uncertainty range of 22–26 Wm^{-2} for the reflected surface solar radiation.

The best estimates for the downward and absorbed surface solar radiation portrayed here are fairly low compared to many of the published estimates. They are, however, in agreement with the corresponding values given in Trenberth et al. (2009), who give best estimates of 184 and 161 Wm^{-2} for downward and absorbed surface solar radiation, respectively. This is remarkable as our estimates are derived completely independently from Trenberth et al. (2009). They used for their estimate the global mean surface solar radiation calculated in the International Satellite Cloud Climatology Project (ISCCP FD) and made an adjustment for underestimated water vapor absorption according to Kim and Ramanathan (2008). On the other hand they did not explicitly take into account any surface observational references. The present study thus gives independent support with direct observations for a comparatively low global mean value of downward and absorbed solar radiation near 185 and 161 Wm^{-2}, respectively. A lower value for the global mean downward solar radiation than typically displayed in energy balance diagrams has been advocated over many years by Ohmura and Gilgen (1993) and Wild et al. (1998).

5.3 Atmospheric solar absorption

Combining our best estimates of TOA and surface absorbed solar radiation in Fig. 1, 240 and 161 Wm^{-2}, respectively, leaves an amount of 79 Wm^{-2} as a residual for the absorption of solar radiation in the atmosphere. This amount coincides with the independent estimate given by Kim and Ramanathan (2008), who integrated global data sets for aerosols, cloud physical properties, and radiation fluxes with a Monte Carlo Aerosol-Cloud-Radiation (MACR) model to determine an atmospheric solar absorption of 79 Wm^{-2}. The uncertainty range for the atmospheric solar absorption given in Fig. 1 is larger than for the other components, since, determined as a residual, the uncertainty ranges of the surface (12 Wm^{-2}) and TOA (5 Wm^{-2}) solar absorption are additive. The CMIP5 models calculate on average an atmospheric solar absorption, which is 5 Wm^{-2} lower than the best estimate obtained here (Table 3), indicative of a too transparent atmosphere causing the excessive surface solar radiation in these models, a feature known also from earlier model assessments (see Sect. 4.2.1).

5.4 Surface thermal fluxes

For the global mean downward thermal radiation, the best estimate of 342 Wm^{-2} derived in Sect. 4.2.2 is used in Fig. 1. This value is higher than found in some other publications such as used in the 3rd and 4th IPCC assessment reports (based on Kiehl and Trenberth 1997). The estimates in Kiehl and Trenberth (1997) (324 Wm^{-2}) and Trenberth et al. (2009) (333 Wm^{-2}), lower by 10–20 Wm^{-2} than obtained here, were not directly determined, but derived as residual terms in the surface energy balance equation. They may therefore be susceptible to uncertainties in the other surface energy balance components. Since these residuals were estimated on a global mean basis, they cannot be directly evaluated against surface observations. A higher value for the downward thermal radiation recently got independent support from studies based on novel space-born active-sounding measurements, which incorporate radar/lidar-derived cloud profiles and associated cloud-base heights. These are critical for an accurate calculation of the downward thermal radiation (Kato et al. 2011; Stephens et al. 2012a, b, Kato et al., in press). These sophisticated satellite-based calculations now independently advocate a higher value, of 344 Wm^{-2} in their latest version (Surface EBAF Ed2.6r, Kato et al. in press), in line with the findings in the present study. As with the downward solar radiation, our approach based on constraints from surface observations is consistent with this latest, completely independent, satellite-derived estimate to within 2 Wm^{-2}.

Also earlier satellite-derived estimates exceeded 340 Wm^{-2}, ranging from 342 to 348 Wm^{-2} (Stephens et al. 2012a). For example, Zhang et al. (2004) determined a global mean downward thermal radiation of 345 Wm^{-2} based on ISCCP-FD, with a mean positive bias of 2.2 Wm^{-2} compared to BSRN observations available at the time, thus also supporting a value very close to the best estimate determined here. Finally, also the reanalyses from the European Center for Medium Range Weather Prediction, ERA Interim and ERA-40, calculate, at 341 and 344 Wm^{-2}, values in close agreement with the best estimate derived in the present study (Berrisford et al. 2011). These reanalyses include the Rapid Radiation Transfer Model (RRTM, Mlawer et al. 1997), which was shown to substantially reduce biases against surface observations when used in a climate model (Wild and Roeckner 2006). They also include the possibly best available estimates of atmospheric temperature and humidity profiles, which should further support an accurate calculation of downward thermal radiation. The biases in the ERA40 downward thermal radiation compared to the BSRN sites are accordingly small (cf. Sect. 4.2.2; Fig. 11, right).

Independently, Ohmura (2012) estimated the global mean downward thermal radiation from BSRN observations at 345 Wm^{-2} at sea level, corresponding to a slightly lower value on real topography, in line with the estimate derived here.

An uncertainty range is also attached to the downward thermal radiation in Fig. 1. As a lower bound for the

uncertainty range, a value of 338 Wm^{-2} is chosen, which corresponds to the CMIP5 multimodel mean downward thermal radiation (Table 3). This is justified following the same line of arguments as above for solar radiation. This study demonstrates that the models show a tendency to underestimate the downward thermal radiation and, as a conservative assumption, there is at least no indication that the models overall would overestimate this quantity. Arguments for a lower value than the multimodel mean of 338 Wm^{-2} are therefore hardly sustainable. We estimate the uncertainty range for this flux to be of similar magnitude as for the downward solar flux, i.e. at 10 Wm^{-2}. This is also justified as no systematic spatial or seasonal dependencies in the model biases are evident which could enlarge the uncertainties. Thus, an upper bound for the uncertainty range of 348 Wm^{-2} is obtained, which also encompasses the highest model value given in Table 3 and Fig. 13, as well as the highest satellite-derived estimates. This upper bound is also justified, as higher values of downward thermal radiation would make a proper closure of the surface energy balance, and with it a realistic intensity of the hydrological cycle, difficult (see discussion below).

The upward thermal flux from the surface can be more straightforward determined than the downward flux discussed above and is less controversial, as it essentially requires the knowledge on the distribution of surface temperature and the Stefan–Boltzman law. Accordingly, the CMIP5 models show a considerably lower variance in the global mean upward thermal fluxes (standard deviation 2.5 Wm^{-2}) than in the downward fluxes (standard deviation 4.8 Wm^{-2}), despite the larger absolute values of the upward component. The multimodel mean and median upward thermal radiation calculated by these climate models are both close to 397 Wm^{-2} (Table 3). We adopted this value of 397 Wm^{-2} for the global mean upward thermal flux in Fig. 1, which lies in between the values of Trenberth et al. (2009) (396 Wm^{-2}), and Stephens et al. (2012b) (398 Wm^{-2}). The value of 397 Wm^{-2} is also close to the upward thermal flux calculated in the ERA40 and ERA Interim (at 398 Wm^{-2}) (Berrisford et al. 2011), and matches the fluxes determined in the National Center for Environmental Prediction (NRA) and the Japanese (JRA) reanalyses (Trenberth et al. 2009).

Uncertainties in this flux should not be more than about 6 Wm^{-2} considering the derivative of the Stephan–Boltzman law and an uncertainty of no more than 1 °C in the underlying surface temperature. The associated uncertainty range in Fig. 1 from 394 to 400 Wm^{-2} covers all major published values as well as most CMIP5 models. Some uncertainty might be introduced in the determination of the upward thermal flux through the specification of the surface emissivity ε, a value close to 1. However, this flux is not overly sensitive to the exact choice of ε, since, if ε is chosen to be lower than 1, the associated reduction in the upward thermal flux is largely compensated for by an additional upward component, stemming from the non-absorbed (upward reflected) part of the downward thermal radiation.

5.5 Surface net radiation

From the best estimates for the thermal exchanges in Fig. 1 (397 Wm^{-2} up, 342 Wm^{-2} down) a net surface thermal cooling of −55 Wm^{-2} can be inferred. Together with the best estimate for the surface absorbed solar radiation of 161 Wm^{-2} in Fig. 1, this results in a best estimate of 106 Wm^{-2} for the global mean surface net radiation. This is the radiative energy available at the surface to be redistributed amongst the non-radiative surface energy balance components. This value is remarkably close to the multimodel mean value of the GCMs, which amounts to 106.2 Wm^{-2} (Table 3). As shown in the above analysis (Sect. 4.2), the GCMs tend to overestimate the downward solar radiation, and underestimate the thermal downward radiation, but nevertheless may achieve a realistic global mean surface net radiation, through compensational errors in their solar and thermal downward fluxes. The "realistic" global mean surface net radiation in the GCMs (due to error cancellations) typically still enables the simulation of adequate global mean surface temperature and precipitation, which state the climate diagnostics that have obtained most attention in the past. Their successful simulation may have to some extent deemed a more detailed analyses of the surface radiation budget as unnecessary in the past. Note that, however, these error cancellations only operate on a global mean basis, but no longer apply on regional, seasonal, and diurnal levels, deteriorating the simulation of surface climate on these scales.

5.6 Non-radiative surface energy fluxes

The 106 Wm^{-2} net surface radiative energy determined above is predominantly used up by the turbulent fluxes of sensible and latent heat (energy equivalent of evaporation), while a small amount (0.6 Wm^{-2}) is going into the subsurface, predominantly into the oceans, since the planet is not in equilibrium. This residual subsurface heat flux, shown as green arrow in Fig. 1, corresponds in magnitude to the planetary energy imbalance, since the heat capacity of the atmosphere is negligible. We ascribe this residual flux a value of 0.6 Wm^{-2} with a conservative uncertainty range from 0.2 to 1.0 Wm^{-2} for the conditions at the beginning of the twenty first century, to cover the estimates discussed in Sect. 4.1. This leaves 105 Wm^{-2} (rounded) radiative energy for the sensible and latent heat fluxes.

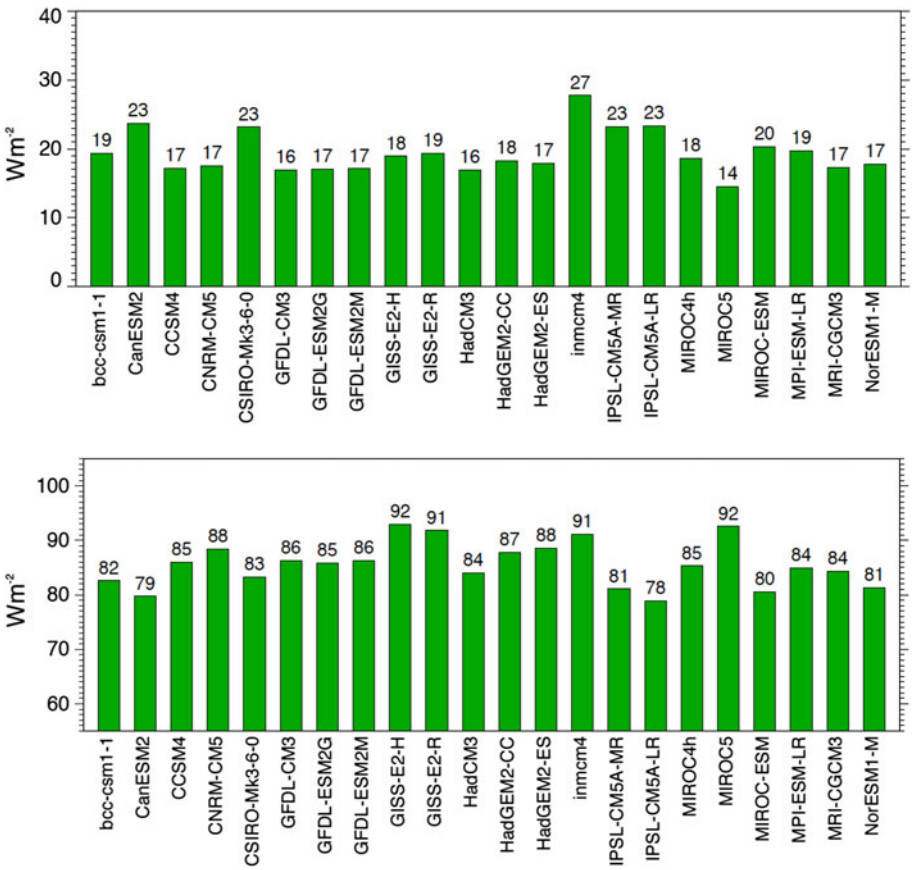

Fig. 19 Global annual mean sensible heat fluxes (*upper panel*) and latent heat fluxes (*lower panel*) at the Earth surface under present day climate as calculated by 22 CMIP5/IPCC AR5 models. Units Wm^{-2}

From all major global energy balance components, the sensible heat flux is the one that is perhaps least constrained by observations. To obtain global mean estimates of this quantity we therefore have to rely largely on modeling studies. The global mean values of the CMIP5 models vary in a range from 15 to 27 Wm^{-2}, with a multimodel mean value slightly below 20 Wm^{-2} (Fig. 19 upper panel; Table 3). The corresponding values from different reanalyses cover a range from 15 to 19 Wm^{-2} (Trenberth et al. 2009; Berrisford et al. 2011). On the other hand, Stephens et al. (2012b) give a best estimate for the sensible heat flux of 24 Wm^{-2}. In Fig. 1 we adopted a value of 20 Wm^{-2} for the global mean sensible heat flux, with an uncertainty range from 15 to 25 Wm^{-2}. This uncertainty range of 10 Wm^{-2} covers the different model and reanalysis estimates as well as the estimate from Stephens et al. (2012b) as upper bound.

In contrast to the sensible heat flux, for the latent heat flux there are observations that have the potential to be used as constraints on a global basis. The latent heat flux is the energy equivalent of the surface evaporation, which on a global mean basis must equal precipitation. Global mean estimates of precipitation may therefore serve as observational constraints for the globally averaged latent heat flux. However, precipitation estimates on a global basis are affected with considerable uncertainties, related to systematic errors in the land-based rain gauge measurements and sampling problems due to the large spatio-temporal variability of this quantity, as well as difficulties inherent in the precipitation retrievals from satellites. Global mean precipitation according to the Global Precipitation Climatology Project (GPCP, Huffman et al. 2009) is estimated at 2.6 mm/day, corresponding to a latent heat flux equivalent of 76 Wm^{-2} (Trenberth et al. 2009). This value has been judged to be too low due to systematic underestimations in the satellite retrievals (Trenberth et al. 2009; Stephens et al. 2012b). The magnitude of these underestimations, however, is currently disputed. Trenberth et al. (2009) accounted for this with an upward adjustment of no more than 5 % to obtain 80 Wm^{-2} for the globally averaged latent heat flux. They also argue that a downward thermal radiation higher than the 333 Wm^{-2} as used in their diagram (and thus $\sim$10 Wm^{-2} lower than supported in the present study) would not be adequate as it would require unrealistically high precipitation and latent heat fluxes to close the surface energy budget. Stephens et al. (2012b) on the other hand argue that the GPCP value is much more underestimated and put their best estimate at 88($\pm$ 10) Wm^{-2}. In Fig. 1 a value of 85 Wm^{-2} is adopted for the global mean latent heat flux, which fits best to our

surface net radiation estimate derived above, considering a sensible heat flux around 20 Wm^{-2}. The 85 Wm^{-2} correspond also to the multimodel mean latent heat flux simulated by the CMIP5 models (Table 3; Fig. 19 lower panel). The realistic global mean surface net radiation in the CMIP5 models (despite the opposing solar and thermal flux biases), implies that also the latent heat flux simulated in these models could be adequate, at least on a global mean basis. 85 Wm^{-2} for the global mean latent heat flux are considered as upper limit of current uncertainties in precipitation retrievals by Trenberth and Fasullo (2012), and at the same time are within the uncertainty range given by Stephens et al. (2012b). The surface sensible and latent heat flux values displayed in Fig. 1 therefore seem to be well-balanced estimates in view of the current controversy on the magnitude of these fluxes and the closure of the energy balance, and are consistent with our best estimate for the available radiative energy at the surface.

The diagram in Fig. 1 is considered to represent present day climate, with the underlying data emphasizing the climatological conditions at the beginning of the twenty first century. One should note that the components of the global energy balance are not necessarily stable over time but may be subject to decadal changes (e.g., Wong et al. 2006; Wild et al. 2009). In terms of the global mean energy balance, changes in individual components are comparatively small compared to the current uncertainties in their absolute amounts. Still, an update of the mean state of the global energy balance will become necessary as time progresses and uncertainty ranges narrow.

6 Concluding remarks

In this study we discussed the global mean energy balance and its representation in the CMIP5 climate models using as much as possible direct observational references from surface stations and space-born platforms. The combination of newly updated observational records and the latest modeling efforts underway for IPCC AR5 allowed us to infer new estimates for the global mean downward surface solar and thermal radiation, which fit best to the surface observations. These estimates enabled also a better quantification of the global mean surface net radiation, which may provide additional constraints on the non-radiative surface energy balance components of sensible and latent heat. These latter components are rather poorly known globally from direct observations and their magnitude is currently debated. We combined the best estimates derived here for the surface radiation budgets with the latest accepted values for the TOA exchanges from recent satellite programs, to derive a new diagram (Fig. 1) representing the global mean energy balance under present day climate conditions at the turn of the millennium. The additional consideration of the information contained in the direct surface observations therein provides a complementary approach to other energy balance estimates which mostly rely on satellite-derived quantities. It is encouraging that our estimates for the global mean downward solar and thermal radiation, which make full use of the surface networks, now coincide within 2 Wm^{-2} with the latest satellite-derived estimates (Kato et al. in press), which are completely independently determined. Uncertainties, however, remain: we consider a 2-sigma uncertainty range on the order of 10 Wm^{-2} still justified for the major surface energy balance components, which is roughly double the corresponding range of the TOA net solar and thermal flux uncertainties. Further progress is required, in terms of extending and expanding high accuracy surface observations, improving surface flux retrievals from satellite products, and refining modeling approaches. Only the combination of all these efforts will ultimately allow to narrow down the uncertainties in the surface energy balance components, not only on a global mean basis, but also on the policy-relevant regional scales.

Acknowledgments This study is supported by the National Centre for Competence in Climate Research (NCCR Climate) of the Swiss National Science Foundation as part of the NCCR Project HyClim. We are grateful to Prof. Atsumu Ohmura for numerous discussions and for his leadership in the establishment of GEBA and BSRN. We highly acknowledge Barbara Schär for the design of the global energy balance figure. We would like to thank Dr. Guido Muller for processing the BSRN data and Dr. Urs Beyerle and Dr. Thierry Corti for all their efforts to download the immense CMIP5 dataset. We acknowledge the international modeling groups for providing their data for analysis, the Program for Climate Model Diagnosis and Intercomparison (PCMDI) for collecting and archiving the model data, the JSC/CLIVAR Working Group on Coupled Modelling (WGCM) and their Coupled Model Intercomparison Project (CMIP) and Climate Simulation Panel for organizing the model data analysis activity, and the IPCC WG1 TSU for technical support. The IPCC Data Archive at Lawrence Livermore National Laboratory is supported by the Office of Science, U.S. Department of Energy. We would like to take this opportunity to acknowledge many hard working site scientists, as listed in http://hdl.handle.net/10013/epic.40092.d001. BSRN data used in this study are available at http://dx.doi.org/10.1594/PANGAEA.792618. We dedicate this study to our dear friend and colleague Ellsworth G. Dutton, who passed away the day this paper was accepted. His enthusiasm and devotion as BSRN project manager over 20 years was invaluable for the success of BSRN.

References

Allan RP, Ringer MA, Pamment JA, Slingo A (2004) Simulation of the Earth's radiation budget by the European Centre for Medium-Range Weather Forecasts 40-year reanalysis (ERA40). J Geophys Res 109:D18107. doi:10.1029/2004JD004816

Anderson DE, Cahalan RF (2005) The solar radiation and climate experiment (SORCE) mission for the NASA earth observing system (eos). Sol Phys 230(1–2):3–6. doi:10.1007/S11207-005-1592-6

Barkstrom BR (1984) The earth radiation budget experiment (ERBE). Bull Am Meteorol Soc 65(11):1170–1185

Berrisford P, Kallberg P, Kobayashi S, Dee D, Uppala S, Simmons AJ, Poli P, Sato H (2011) Atmospheric conservation properties in ERA-interim. Q J Royal Meteorol Soc 137(659):1381–1399. doi:10.1002/Qj.864

Bodas-Salcedo A, Ringer MA, Jones A (2008) Evaluation of the surface radiation budget in the atmospheric component of the hadley centre global environmental model (hadgem1). J Clim 21(18):4723–4748. doi:10.1175/2008jcli2097.1

Chevallier F, Morcrette JJ (2000) Comparison of model fluxes with surface and top-of-the-atmosphere observations. Mon Weather Rev 128(11):3839–3852

Dutton EG (1993) An extended comparison between lowtran7 computed and observed broad-band thermal irradiances—global extreme and intermediate surface conditions. J Atmos Ocean Tech 10(3):326–336

Frohlich C (1991) History of solar radiometry and the world radiometric reference. Metrologia 28(3):111–115

Garratt JR (1994) Incoming shortwave fluxes at the surface—a comparison of gcm results with observations. J Clim 7(1):72–80

Garratt JR, Prata AJ (1996) Downwelling longwave fluxes at continental surfaces—a comparison of observations with gcm simulations and implications for the global land surface radiation budget. J Clim 9(3):646–655

Gilgen H, Wild M, Ohmura A (1998) Means and trends of shortwave irradiance at the surface estimated from global energy balance archive data. J Clim 11(8):2042–2061

Gleckler PJ, Weare BC (1997) Uncertainties in global ocean surface heat flux climatologies derived from ship observations. J Clim 10(11):2764–2781

Gupta SK, Ritchey NA, Wilber AC, Whitlock CH, Gibson GG, Stackhouse PW (1999) A climatology of surface radiation budget derived from satellite data. J Clim 12(8):2691–2710

Gutowski WJ, Gutzler DS, Wang WC (1991) Surface-energy balances of 3 general-circulation models—implications for simulating regional climate change. J Clim 4(2):121–134

Hansen J, Sato M, Kharecha P, von Schuckmann K (2011) Earth's energy imbalance and implications. Atmos Chem Phys 11(24):13421–13449. doi:10.5194/Acp-11-13421-2011

Hartmann DL, Short DA (1980) On the use of earth radiation budget statistics for studies of clouds and climate. J Atmos Sci 37(6):1233–1250

Hartmann DL, Ramanathan V, Berroir A, Hunt GE (1986) Earth radiation budget data and climate research. Rev Geophys 24(2):439–468

Hatzianastassiou N, Vardavas I (1999) The net radiation budget of the northern hemisphere. J Geophys Res Atmos 104(D22): 27341–27359

Hatzianastassiou N, Matsoukas C, Fotiadi A, Pavlakis KG, Drakakis E, Hatzidimitriou D, Vardavas I (2005) Global distribution of Earth's surface shortwave radiation budget. Atmos Chem Phys 5:2847–2867

Huffman GJ, Adler RF, Bolvin DT, Gu GJ (2009) Improving the global precipitation record: Gpcp version 2.1. Geophys Res Lett 36:L17808. doi:10.1029/2009gl040000

Iacono MJ, Mlawer EJ, Clough SA, Morcrette JJ (2000) Impact of an improved longwave radiation model, rrtm, on the energy budget and thermodynamic properties of the ncar community climate model, ccm3. J Geophys Res Atmos 105(D11):14873–14890

Kato S, Rose F, Sun-Mack S, Miller W, Chen Y, Rutan D, Stephens G, Loeb N, Minnis P, Wielicki B, Winker D, Charlock T, Stackhouse P, Xu K, Collins W (2011) Improvements of top-of-atmosphere and surface irradiance computations with calipso-, cloudsat-, and modis-derived cloud and aerosol properties. J Geophys Res 116:D19209. doi:10.1029/2011JD016050

Kato S, Loeb NG, Rutan DA, Rose FG, Sun-Mack S, Miller WF, Chen Y (2012) Uncertainty estimate of surface irradiances computed with modis-, calipso-, and cloudsat-derived cloud and aerosol properties. Surv Geophys 33(3–4):395–412. doi: 10.1007/S10712-012-9179-X

Kato S, Loeb NG, Rose FG, Doelling DR, Rutan DA, Caldwell TE, Yu L, Weller R. Surface irradiances consistent with CERES-derived top-of-atmosphere shortwave and longwave irradiances. J Clim (in press)

Kiehl JT, Trenberth KE (1997) Earth's annual global mean energy budget. Bull Am Meteorol Soc 78(2):197–208

Kim DY, Ramanathan V (2008) Solar radiation budget and radiative forcing due to aerosols and clouds. J Geophys Res Atmos 113(D2):D02203. doi:10.1029/2007jd008434

Kopp G, Lean JL (2011) A new, lower value of total solar irradiance: evidence and climate significance. Geophys Res Lett 38:L01706. doi:10.1029/2010gl045777

Kopp G, Lawrence G, Rottman G (2005) The total irradiance monitor (tim): science results. Sol Phys 230(1–2):129–139. doi: 10.1007/S11207-005-7433-9

Levitus S, Antonov J, Boyer T, Locarnini RA, Garcia HE, Mishonov AV (2009) Global ocean heat content 1955–2008 in light of recently revealed instrumentation problems. Geophys Res Lett 36:L07608. doi:10.1029/2008GL037155

Li ZQ, Moreau L, Arking A (1997) On solar energy disposition: a perspective from observation and modeling. Bull Am Meteorol Soc 78(1):53–70

Loeb NG, Wielicki BA, Doelling DR, Smith GL, Keyes DF, Kato S, Manalo-Smith N, Wong T (2009) Toward optimal closure of the earth's top-of-atmosphere radiation budget. J Clim 22(3): 748–766. doi:10.1175/2008jcli2637.1

Loeb NG, Lyman JM, Johnson GC, Allan RP, Doelling DR, Wong T, Soden BJ, Stephens GL (2012) Observed changes in top-of-the-atmosphere radiation and upper-ocean heating consistent within uncertainty. Nat Geosci 5(2):110–113. doi:10.1038/Ngeo1375

Lyman JM, Good SA, Gouretski VV, Ishii M, Johnson GC, Palmer MD, Smith DM, Willis JK (2010) Robust warming of the global upper ocean. Nature 465(7296):334–337. doi:10.1038/Nature09043

Markovic M, Jones CG, Vaillancourt PA, Paquin D, Winger K, Paquin-Ricard D (2008) An evaluation of the surface radiation budget over North America for a suite of regional climate models against surface station observations. Clim Dyn 31(7–8):779–794. doi:10.1007/s00382-008-0378-6

Marty C, Philipona R, Delamere J, Dutton EG, Michalsky J, Stamnes K, Storvold R, Stoffel T, Clough SA, Mlawer EJ (2003) Downward longwave irradiance uncertainty under Arctic atmospheres: measurements and modeling. J Geophys Res Atmos 108(D12):4358. doi:10.1029/2002jd002937

Mercado LM, Bellouin N, Sitch S, Boucher O, Huntingford C, Wild M, Cox PM (2009) Impact of changes in diffuse radiation on the global land carbon sink. Nature 458(7241):1014–1018. doi: 10.1038/Nature07949

Michalsky J, Dutton E, Rubes M, Nelson D, Stoffel T, Wesley M, Splitt M, DeLuisi J (1999) Optimal measurement of surface shortwave irradiance using current instrumentation. J Atmos Ocean Tech 16(1):55–69

Michalsky JJ, Gueymard C, Kiedron P, McArthur LJB, Philipona R, Stoffel T (2007) A proposed working standard for the measurement of diffuse horizontal shortwave irradiance. J Geophys Res Atmos 112(D16):D16112. doi:10.1029/2007jd008651

Michalsky J, Dutton EG, Nelson D, Wendell J, Wilcox S, Andreas A, Gotseff P, Myers D, Reda I, Stoffel T, Behrens K, Carlund T, Finsterle W, Halliwell D (2011) An extensive comparison of commercial pyrheliometers under a wide range of routine observing conditions. J Atmos Ocean Tech 28(6):752–766. doi: 10.1175/2010jtecha1518.1

Mlawer EJ, Taubman SJ, Brown PD, Iacono MJ, Clough SA (1997) Radiative transfer for inhomogeneous atmospheres: Rrtm, a validated correlated-k model for the longwave. J Geophys Res Atmos 102(D14):16663–16682

Morcrette JJ (2002) Assessment of the ecmwf model cloudiness and surface radiation fields at the arm sgp site. Mon Weather Rev 130(2):257–277

Ohmura A (2012) Present status and variations in the Arctic energy balance. Polar Sci 6:5–13

Ohmura A, Gilgen H (1993) Reevaluation of the global energy-balance. Interact Between Glob Clim Subsyst 75:93–110

Ohmura A, Gilgen H, Wild M (1989) Global energy balance archive GEBA, world climate program—water project a7. Zuercher Geografische Schriften 34. Zuerich

Ohmura A, Dutton EG, Forgan B, Frohlich C, Gilgen H, Hegner H, Heimo A, Konig-Langlo G, McArthur B, Muller G, Philipona R, Pinker R, Whitlock CH, Dehne K, Wild M (1998) Baseline surface radiation network (bsrn/wcrp): new precision radiometry for climate research. Bull Am Meteorol Soc 79(10):2115–2136

Ohmura A, Bauder A, Muller H, Kappenberger G (2007) Long-term change of mass balance and the role of radiation. Ann Glaciol 46:367–374

Philipona R, Dutton EG, Stoffel T, Michalsky J, Reda I, Stifter A, Wendling P, Wood N, Clough SA, Mlawer EJ, Anderson G, Revercomb HE, Shippert TR (2001) Atmospheric longwave irradiance uncertainty: pyrgeometers compared to an absolute sky-scanning radiometer, atmospheric emitted radiance interferometer, and radiative transfer model calculations. J Geophys Res Atmos 106(D22):28129–28141

Pinker RT, Frouin R, Li Z (1995) A review of satellite methods to derive surface shortwave irradiance. Remote Sens Environ 51(1):108–124

Potter GL, Cess RD (2004) Testing the impact of clouds on the radiation budgets of 19 atmospheric general circulation models. J Geophys Res Atmos 109(D2):D02106. doi:10.1029/2003jd004018

Qian Y, Long CN, Wang H, Comstock JM, McFarlane SA, Xie S (2012) Evaluation of cloud fraction and its radiative effect simulated by IPCC AR4 global models against ARM surface observations. Atmos Chem Phys 12(4):1785–1810. doi:10.5194/Acp-12-1785-2012

Ramanathan V, Cess RD, Harrison EF, Minnis P, Barkstrom BR, Ahmad E, Hartmann D (1989) Cloud-radiative forcing and climate—results from the Earth radiation budget experiment. Science 243(4887):57–63

Ramanathan V, Crutzen PJ, Kiehl JT, Rosenfeld D (2001) Atmosphere—aerosols, climate, and the hydrological cycle. Science 294(5549):2119–2124

Raschke E, Ohmura A (2005) Radiation budget of the climate system. In: Hantel M (ed) Observed global climate vol 6. Landolt-börnstein—group v geophysics, numerical data and functional relationships in science and technology. Springer, Berlin, pp 25–46. doi:10.1007/b75667

Roesch A, Wild M, Ohmura A, Dutton EG, Long CN, Zhang T (2011) Assessment of bsrn radiation records for the computation of monthly means. Atmos Meas Tech 4(2):339–354. doi:10.5194/Amt-4-339-2011

Stephens GL, Wild M, Stackhouse P, L'Ecuyer T, Kato S (2012a) The global character of the flux of downward longwave radiation. J Clim 25:2329–2340. doi:10.1175/JCLI-D-11-00262.1

Stephens GL, Li JL, Wild M, Clayson CA, Loeb N, Kato S, L'Ecuyer T, Stackhouse PW, Andrews T (2012b) The energy balance of the earth's climate system. Nat Geosci 5:691–696. doi:10.1038/ngeo1580

Trager-Chatterjee C, Muller RW, Trentmann J, Bendix J (2010) Evaluation of ERA-40 and ERA-interim re-analysis incoming surface shortwave radiation datasets with mesoscale remote sensing data. Meteorol Z 19(6):631–640. doi:10.1127/0941-2948/2010/0466

Trenberth KE, Fasullo JT (2010) Simulation of present-day and twentyfirst-century energy budgets of the Southern Oceans. J Clim 23:440–454

Trenberth KE, Fasullo JT (2012) Tracking earth's energy: from El Nino to global warming. Surv Geophys 33(3–4):413–426. doi:10.1007/S10712-011-9150-2

Trenberth KE, Fasullo JT, Kiehl J (2009) Earth's global energy budget. Bull Am Meteorol Soc 90(3):311. doi:10.1175/2008bams2634.1

Uppala SM, Kallberg PW, Simmons AJ, Andrae U, Bechtold VD, Fiorino M, Gibson JK, Haseler J, Hernandez A, Kelly GA, Li X, Onogi K, Saarinen S, Sokka N, Allan RP, Andersson E, Arpe K, Balmaseda MA, Beljaars ACM, Van De Berg L, Bidlot J, Bormann N, Caires S, Chevallier F, Dethof A, Dragosavac M, Fisher M, Fuentes M, Hagemann S, Holm E, Hoskins BJ, Isaksen L, Janssen PAEM, Jenne R, McNally AP, Mahfouf JF, Morcrette JJ, Rayner NA, Saunders RW, Simon P, Sterl A, Trenberth KE, Untch A, Vasiljevic D, Viterbo P, Woollen J (2005) The ERA-40 re-analysis. Q J Royal Meteorol Soc 131(612):2961–3012. doi:10.1256/Qj.04.176

Wielicki BA, Barkstrom BR, Harrison EF, Lee RB, Smith GL, Cooper JE (1996) Clouds and the earth's radiant energy system (CERES): an earth observing system experiment. Bull Am Meteorol Soc 77(5):853–868

Wild M (2005) Solar radiation budgets in atmospheric model intercomparisons from a surface perspective. Geophys Res Lett 32(7):L07704. doi:10.1029/2005gl022421

Wild M (2008) Short-wave and long-wave surface radiation budgets in GCMs: a review based on the IPCC-AR4/CMIP3 models. Tellus A 60(5):932–945. doi:10.1111/J.1600-0870.2008.00342.X

Wild M (2012) New directions: a facelift for the picture of the global energy balance. Atmos Environ 55:366–367. doi:10.1016/j.atmosenv.2012.03.022

Wild M, Roeckner E (2006) Radiative fluxes in the ECHAM5 general circulation model. J Clim 19(16):3792–3809

Wild M, Schmucki E (2011) Assessment of global dimming and brightening in IPCC-AR4/CMIP3 models and era40. Clim Dyn 37(7–8):1671–1688. doi:10.1007/S00382-010-0939-3

Wild M, Ohmura A, Gilgen H, Roeckner E (1995a) Regional climate simulation with a high-resolution GCM—surface radiative fluxes. Clim Dyn 11(8):469–486

Wild M, Ohmura A, Gilgen H, Roeckner E (1995b) Validation of general-circulation model radiative fluxes using surface observations. J Clim 8(5):1309–1324

Wild M, Ohmura A, Gilgen H, Roeckner E, Giorgetta M, Morcrette JJ (1998) The disposition of radiative energy in the global climate system: GCM-calculated versus observational estimates. Clim Dyn 14(12):853–869

Wild M, Ohmura A, Gilgen H, Morcrette JJ, Slingo A (2001) Evaluation of downward longwave radiation in general circulation models. J Clim 14(15):3227–3239

Wild M, Long CN, Ohmura A (2006) Evaluation of clear-sky solar fluxes in GCMs participating in AMIP and IPCC-AR4 from a surface perspective. J Geophys Res Atmos 111(D1):D01104. doi:10.1029/2005jd006118

Wild M, Grieser J, Schaer C (2008) Combined surface solar brightening and increasing greenhouse effect support recent intensification of the global land-based hydrological cycle. Geophys Res Lett 35(17):L17706. doi:10.1029/2008gl034842

Wild M, Truessel B, Ohmura A, Long CN, Konig-Langlo G, Dutton EG, Tsvetkov A (2009) Global dimming and brightening: an

update beyond 2000. J Geophys Res Atmos 114:D00d13. doi:10.1029/2008jd011382

Wong T, Wielicki BA, Lee RB, Smith GL, Bush KA, Willis JK (2006) Reexamination of the observed decadal variability of the earth radiation budget using altitude-corrected ERBE/ERBS nonscanner wfov data. J Clim 19(16):4028–4040

Zhang YC, Rossow WB, Lacis AA, Oinas V, Mishchenko MI (2004) Calculation of radiative fluxes from the surface to top of atmosphere based on ISCCP and other global data sets: refinements of the radiative transfer model and the input data. J Geophys Res Atmos 109(D19):D19105. doi:10.1029/2003jd004457